This is a non-peer reviewed manuscript preprint submitted to EarthArXiv. This paper has been submitted to Sedimentology. The authors welcome feedback on this article.

Fluvial response and recovery after the Permo-Triassic Mass Extinction revealed through quantitative paleohydrology

Xiang Yan, Alexander C. Whittaker and Gary J. Hampson*

Department of Earth Science and Engineering, Imperial College London, London SW7 2AZ, UK

***Correspondence:** Xiang.yan19@imperial.ac.uk

Abstract

Anthropogenic climate change represents the greatest modern forcing on global river dynamics. Investigating the sensitivity of rivers to past climate in the geological record is thus crucial in understanding future landscapes in a warming world. The Sherwood Sandstone Group, UK, a unit of early-middle Triassic (c. 248-239 Ma) dryland fluvial deposits, records events during and after the Permo-Triassic Mass Extinction. We quantify the evolution of this fluvial system, exposed in the southwest UK, by combining facies-scale sedimentology with a numerical paleohydrologic workflow. We reconstruct key hydraulic and geomorphic characteristics, showing that gravel-bed lower Triassic rivers had paleoslopes between 1.0×10^{-3} and 2.0×10^{-3} m/m and bankfull water discharges of 760-810 m^3/s. During the middle Triassic, rivers were sand-bedded, with paleoslopes between 8×10^{-4} and 5×10^{-4} m/m. Bankfull water discharges ranged between 380 and 480 m^3/s: half those of the lower Triassic. This halving of bankfull discharge occurs despite an inferred eightfold increase in catchment area in the mid-Triassic and stable levels of long-term precipitation, indicating that catchments in the lower Triassic were generating highly intermittent, disproportionately large bankfull flow events. Coupled with the abnormally coarse grain size recorded in the Lower Triassic and regional stratigraphic correlations to similar deposits across NW Europe, we attribute this to a global hyperthermal event: the Late Smithian Thermal Maximum (c. 248 Ma). Rapid warming during a greenhouse interval triggered widespread landscape devegetation and bedrock erosion, and extreme, infrequent monsoonal precipitation. Our results demonstrate the ability of quantitative paleohydrology to produce numerically-informed depositional models, and identify the impacts of global warming during the greatest biotic-climatic turnover of the Phanerozoic.

1. Introduction

Fluvial stratigraphy provides a valuable archive of landscape response to environmental and tectonic forcings in the geological past (Armitage et al., 2011; Romans et al., 2016; Castelltort et al., 2023. Rivers are highly sensitive to climate change through their discharge regime (e.g. Larkin et al., 2020; Satoh et al., 2022; McLeod et al., 2024, Wang et al., 2024), so understanding how ancient fluvial systems responded to and recorded these drivers is of key importance for constraining the impact of future climate change, given that 1.5-4.5°C of anthropogenic global warming is forecasted by 2100 (Meinshausen et al., 2011; Van Vuuren et al., 2026), Globally, drylands are the largest continental ecosystem by area, covering 40% of the Earth's land surface, and support a third of the global population

(Millennium Ecosystem Assessment, 2005; Safriel et al., 2005) so constraining the behaviour of dryland rivers in the geological record is particularly crucial for addressing landscape sensitivity to climate.

Internationally, dryland fluvial deposits also serve as important reservoir units for geothermal energy and the geological storage of carbon dioxide, both key components of the energy transition (e.g. Schellschmidt et al., 2010; Mijnlieff, 2020; Hjelm et al., 2020; English et al., 2024; Gasanzade and Bauer, 2025). A better understanding of the dynamics of fluvial systems thus also allows us to build improved depositional models for these reservoirs (e.g. Lang et al., 2004; Menacherry et al., 2009; McKie, 2011; Morón et al., 2014; Newell and Shariatipour, 2016; Henares et al., 2020; Hossain et al., 2024).

Facies-based sedimentological analysis can be an effective tool to understand the dynamics of past fluvial systems (e.g. Blum and Törnqvist, 2000; Miall, 2006; Colombera et al., 2013; Plink-Björklund et al., 2015; Fielding et al., 2018). However, dryland fluvial deposits are often biotically sparse or barren, limiting the availability of chronostratigraphic and climate proxy data, which is crucial in inferring external forcings. Yet, paleohydraulic methods, which use direct measurements of the preserved stratigraphic record, such as grain size and the thickness and distribution of cross-strata, can reconstruct fluvial behaviour, and have increasingly offered the potential to quantify river dynamics in the geological past (e.g. Leclair and Bridge, 2001; Trampush et al., 2014; Bradley and Venditti, 2017; Long et al., 2021). In principle, these methods enable us to go further than insights from facies-based analyses alone, particularly when such approaches are combined carefully with descriptive and qualitative observations from stratigraphy (e.g. Bhattacharya et al., 2016; Lyster et al., 2021; Wood et al., 2022; 2025; Sharma et al., 2023; McLeod et al., 2023; 2025; Valenza et al., 2026).

The Sherwood Sandstone Group (SSG) of the British Isles is a regionally significant unit of Triassic fluvial and aeolian sandstones, deposited in central Pangea at low latitudes in a dryland setting (**fig. 1a, b)** (c. 250 to 239.6 Ma, Yan et al., 2026). The SSG is a significant reservoir unit for geothermal energy (Downing et al., 1984; Moscardini et al., 2025; Brémaud et al., 2026), the geological storage of carbon dioxide (e.g. Chedburn et al., 2022; English et al., 2024; Hossain et al., 2024; Breeze et al., 2026) and groundwater resources in the UK (e.g. Plant et al., 1999; Newell and Smith, 2009; Medici et al., 2019). The SSG is also holds particular climatic significance, as it records the Permo-Triassic Mass Extinction and its aftermath (e.g. Bourquin et al., 2011; Radley and Coram, 2016; Newell, 2017b). The SSG hence serves both as a key unit of interest for the energy transition, as well as preserving a record of the most extreme climatic-biotic turnover of the Phanerozoic (Benton and Newell, 2014; Radley and Coram, 2016; Newell, 2017a; b).

A complete section of the SSG crops out on the south coast of Devon in the southwest UK, at the western edge of the Wessex Basin (**fig. 1b, c**). Owing to the continuity and quality of outcrop, the SSG here has a long history of characterisation (e.g. Smith, 1990; Smith and Edwards, 1991; Hounslow and McIntosh, 2004; Morton et al., 2013; Newell, 2017b; Hounslow and Gallois, 2023). Thus, the Devon coastal section represents an ideal location to apply quantitative paleohydraulic methods to quantify the changing fluvial character of a dryland system through the lower to middle Triassic.

Here, we first reconstruct the paleohydraulic character of the rivers of the SSG using a quantitative palaeohydrological framework for the first time. Combined with the results of facies-based sedimentology, we derive parameters such as river paleoslope, planform, bankfull water discharge and bankfull sediment flux to produce updated, quantitatively informed depositional models, referenced against modern rivers. Secondly, we evaluate the climatic forcings behind the changing character of fluvial deposition in the SSG, especially in relation to the Permo-Triassic Mass Extinction and its recovery period.

2. Geological and paleoclimatic setting

The SSG was deposited in a series of linked, extensional basins formed during the initial phase of supercontinent breakup (e.g. Bourquin et al., 2011; McKie, 2017). The SSG overlies the existing Permian basin fill, and underlies the Mercia Mudstone Group, a unit of playa and lacustrine mudstones (e.g. Howard et al., 2008; Newell, 2024). The SSG is composed of the Chester Formation (CHF), the Wilmslow Sandstone Formation and the Helsby Sandstone Formation (HSF) (Ambrose et al., 2014). The CHF and HSF were deposited by two, long-distance, north-flowing river systems (**fig. 1,** e.g. Tyrrell et al., 2012; Morton et al., 2013; 2016; Franklin et al., 2020) with distinct source areas and sedimentological character (Morton et al., 2016, Yan et al., 2026). On the source-to-sink scale, the rivers of the CHF have previously been designated as the ‘Sherwood 1 River System’, and the rivers of the HSF designated as the ‘Sherwood-2 River System’ (Yan et al., 2026).

In Devon, the CHF is approximately 30 m thick and conglomeratic (Smith, 1990; Smith and Edwards, 1991). The HSF is approximately 200 m thick and is dominated by sandstone (Newell, 2017b). The CHF and HSF are separated by a paleosol horizon and an aeolian deflation surface (e.g. Leonard et al., 1982; Wright et al., 1991) which represents the Mid-Triassic Unconformity (*sensu* Newell, 2017b), and the Wilmslow Sandstone Formation is absent. In older, local lithostratigraphic nomenclature, the CHF is known as the Budleigh Salterton Pebble Beds, and the HSF as the Otter Sandstone (Ambrose et al., 2014). In Devon, the change in sediment routing between the Sherwood-1 (CHF) and Sherwood-2 river systems (HSF) manifests as a substantial expansion in catchment area for the rivers of the HSF compared to those of the CHF, inferred from quantitative provenance analysis (**fig. 1b**, Morton et al., 2013). This regional drainage reorganisation was likely driven by the Hardegsen tectonic event (Bourquin et al., 2011; von Eynatten et al., 2026).

Though not formally divided into lithostratigraphic members, the CHF can be divided into two architecturally distinct units, representing rivers of differing fluvial character (**fig. 2;** Smith, 1990; Smith and Edwards, 1991). The HSF has a well-defined lithostratigraphy, and is divided into four members. Each member is bounded by major erosion surfaces, and possesses distinct sedimentological, geochemical and heavy mineral characteristics (Morton et al., 2013; Newell, 2017b). The lowermost unit of the HSF is the 15 m thick aeolian West

Down Member (**fig. 2**), which is restricted to the Devon coastal section (Smith and Edwards, 1991; Newell, 2017b). The overlying succession is dominantly fluvial, and comprises the Otterton Ledge, Chiselbury Bay and Pennington Point members, which are c. 115 m, 50 m and 20 m thick, respectively (Newell, 2017b). Previous interpretations of fluvial planform have been made from sedimentary architectural analysis, suggesting that the majority of the SSG was deposited by braided rivers in accordance with the multistorey, multilateral channel-fill sandstone complexes which dominate the unit (e.g. Sellwood et al., 1984; Purvis and Wright, 1991; Newell, 2017b; Coram et al., 2019).

Though the chronology of the CHF is not fully constrained, regional stratigraphic correlations suggest that the CHF is of Smithian Age in the Olenekian Stage of the lower Triassic (**fig. 2**, c. 250 – 248 Ma, Bourquin et al., 2011). During this time, continued activity from the Siberian Traps Large Igneous Province resulted in prolonged global climatic instability after the onset of the Permo-Triassic Extinction at 251.9 Ma (Ogg et al., 2020). This resulted in a fluctuating but consistently hyperthermal climate, as reflected in the global $\delta^{13}C$ isotope record (**fig. 2,** Sun et al., 2012; Benton and Newell, 2014). The age of the CHF overlaps with the Late Smithian Thermal Maximum, the final and most extreme hyperthermal of the lower Triassic, with peak continental temperatures of 35-40°C (Sun et al., 2012), and significant perturbations to the global biosphere (Sun et al., 2012; Linström et al., 2019). Although climate in general has been suggested as a driver for the deposition of the CHF (Radley and Coram, 2016; Newell, 2017a), alternate forcings, such as tectonic activity (Wills, 1956) and more proximal sediment sourcing (Wills, 1970; Burgess et al., 2025) have also been proposed to account for the coarse grain size of this unit.

The chronology of the mid-Triassic HSF is well-constrained using magnetostratigraphy (**fig. 2,** Yan et al., 2026). The Otterton Ledge Member has a duration of 5.3 Ma (246.5-241.2 Ma, including the West Down Member), the Chiselbury Bay Member spans 1 Myr (241.2-240.2 Ma), and the Pennington Point Member represents 0.6 Myr (240.2-239.6 Ma) (**fig. 2**). By this time, the cessation of the Siberian Traps Large Igneous Province allowed the climate to stabilise and the biosphere to recover (**fig. 2,** Newell, 2017a), reflected in the abundance of vegetation, and the biotic diversity of fossils in the study area (Benton and Spencer, 1995; Newell, 2017b; Coram et al., 2019).

The boundary between the HSF and the mid- to late-Triassic Mercia Mudstone Group is strongly diachronous across the British Isles (e.g. Hounslow and Gallois, 2023; Yan et al., 2026). This diachroneity represents a north-to-south transgression of Mercia Mudstone Group playa lake facies and a resultant shortening of the Sherwood-2 River System, and coincides with a regional aridification coincident with the Muschelkalk transgression (Bourquin et al., 2011; McKie, 2017; Newell, 2017a).

3. Methods

3.1. Overview of primary data collection and workflow

Our data collection and workflow is summarised in **fig. 3**, with data and extended methods in **Supplementary Material 1, 2**. Primary field data for palaeohydrological analysis include dune-scale measurements of cross bedding, barform-scale architectural measurements, bar accretion direction (**e.g. figs. 4, 5**), and measurements of sediment grain size (**e.g. figs. 6a, b**). Field data were collected from a total of 16 localities in Devon (**figs. 1c, 2**): 4 localities for the CHF (**figs. 4a-f)** and 12 localities for the HSF (**figs. 5a-f**), and are sedimentologically representative of each member of the SSG. The data collection approach and the paleohydraulic workflow used in this study build on those established by Ganti et al. (2019), Lyster et al. (2021), Wood et al. (2022), and McLeod et al. (2025). Here we contextualise these paleohydraulic data with outcrop-based observations of facies and architectural elements; these observations complement previous facies analyses (Smith, 1990; Smith and Edwards, 1991; Lorsong and Atkinson, 1995; McKie and Williams, 2009; Newell, 2017b).

Measurements were made of maximum dune-scale cross-set thickness (n = 377) and cross-set thickness distributions (n = 51, **figs. 4f, 5h**) as these measurements enable us to constrain typical subaqueous bedform sizes in the SSG, which can be quantitatively linked to palaeoflow depths. Measurements were also made of cross-set lee face dip and dip direction to constrain palaeocurrents (n = 231, **figs. 4f; 5h**). Cross-set thicknesses were measured to a precision of 10 mm, with thickness distributions containing ca. 10 evenly spaced measurements per cross-set. From cross-set distributions, the scaling relationship between mean and maximum cross-set thickness could then be derived. Maximum cross-set thicknesses were then transformed into synthetic mean thicknesses using this scaling factor, increasing the total number of mean thicknesses to n = 428. Mean thicknesses were then incorporated into the paleohydraulic workflow to calculate bankfull flow depths, using the scaling relationships of Leclair and Bridge (2001) and Bradley and Venditti (2017), with a Monte-Carlo approach to propagate uncertainty (c.f. Lyster et al., 2021) (**fig. 3, Section 3.2**).

Architectural observations and measurements were made of fluvial bars and simple channel-fill elements. In the SSG, barforms are often laterally and vertically amalgamated (**figs. 4a-d, 5a-e**), but can be recognised by inclined, low-angle accretion surfaces, often with superimposed higher angle dune cross-bedding (**figs. 4e, 5g, h**). The maximum thicknesses of bars and channel-fill architectural elements (n = 41) provide an independent constraint on minimum bankfull flow depth. Bar and channel-fill thicknesses were also measured using published, interpreted architectural panels (Localities A, B in **fig. 1a, 2,** Lorsong and Atkinson, 1995; Newell and Shariatipour, 2016), and from one cliff section at Danger Point (locality 7, **fig. 1a**). Measurements were also made of the dip and dip direction of barform accretion surfaces (n = 97). When combined with paleocurrent measurements, the accretionary style of bars (downstream, lateral and upstream) could be determined (c.f. Valenza et al., 2026). Rarely, the length of inclined, barform lateral-accretion surfaces could be traced laterally and measured (n = 2) to provide constraints on bankfull channel width (Greenburg et al., 2022). All barform-scale architectural-element measurements of thickness and length were made using a laser range finder to a precision of 0.1 m.

Median grain size (D_{50}) was measured for both gravel-grade and sand-grade sediment (**figs. 6a, b**). For sandstone-dominated packages (D_{50} < 2 mm), D_{50} was measured using the grain-size classification of Wentworth (1922) (n = 67). For conglomeratic packages (D_{50} > 2 mm), D_{50} was obtained by measuring the long axis of clasts using the method of Wolman (1954). Measurements of gravel-grade sediment were made to a precision of 1 mm, both in the field and from outcrop photographs (n = 19, 100 measurements each). Median grain size, along with calculated bankfull flow depths, was incorporated into the paleohydraulic workflow to calculate paleoslope (Trampush et al., 2011) (**fig. 3, section 3.3**).

3.2. Reconstruction of bankfull flow depth and slope

Dune-scale cross-set and barform-scale architectural-element thickness data for the SSG were decompacted using the procedure of Long (2021), using a mean compaction factor of 1.16 calculated from 14 individual thin sections collected from the field area (Burley 1987). Grain size data, along with decompacted cross-set and architectural-element thickness data, were then grouped by lithostratigraphic division. This grouping allows temporal changes in paleohydraulic character to be appraised.

For each lithostratigraphic division, dune-scale thickness, architectural-element-scale thickness and grain size data were passed through a series of scaling relationships to derive successive paleohydraulic parameters. Where relationships have stated uncertainties, a Monte Carlo uncertainty propagation was used to produce statistically robust results, with 10^5 outcomes modelled with a rectangular distribution within the bounds of respective uncertainties.

Firstly, original dune heights (h_d) were calculated from mean decompacted cross-set thicknesses (h_{xs}), using **Equation 1** (Leclair and Bridge, 2001), where h_d is a function of h_{xs}. This equation is ultimately derived from the theoretical work of Paola and Borgman (1991), and is appropriate for bedforms migrating over random topography with a negligible angle of climb.

$$h_d = (2.9 \pm 0.7)h_{xs} \quad \textbf{(1)}$$

Bankfull flow depths (*H*) were calculated the reconstructed dune heights using a compilation of flume tank and observational data from sand bed modern rivers (Equation 2) (Bradley and Venditti, 2017).

$$H = (6.7^{+3.4}_{-2.3})h_d \quad \textbf{(2)}$$

H was also independently reconstructed from the maximum decompacted vertical thicknesses of accretionary barform and simple channel-fill architectural elements (h_{bar}). Bars in the SSG are often vertically amalgamated and truncated, so values of *H* represent minimum estimates (**fig. 4a-d, fig. 5a-e**). The results of barform and dune-scale approaches were then compared to ensure that results were consistent and geologically reasonable.

Paleoslopes (*S*, m/m) were calculated using the relationship of Trampush et al. (2014) (**Equation 3**), which in effectis a semi-empirical solution for bankfull Shields stress as a function of particle Reynolds number. Here, *S* is expressed a function of *H* and D_{50}, with parameters derived using a global database of both sand- and gravel-bed modern rivers.

$$\log S = (-2.08 \pm 0.036) + (0.254 \pm 0.016)\log D_{50} + (-1.09 \pm 0.044)\log H \quad \textbf{(3)}$$

3.3. Constraining fluvial planform and width

Constraints on total active channel width, *W*, are important for the paleohydraulic workflow, as width is commonly used in interpreting channel planform (Parker, 1976; Ganti et al., 2019; Lyster et al., 2022; Wood et al., 2022; McLeod et al., 2025). *W* is also required to obtain total bankfull water and sediment flux values for sediment routing system reconstruction. However, *W* cannot be directly measured as the SSG is largely composed of channel-fill bodies that are incompletely preserved due to erosional truncation within multistorey, multilateral channel-fill complexes. Considering this uncertainty, we reconstruct fluvial planform from both paleohydraulic methods and from facies and architectural observations. We then reconstruct plausible values of *W* for each stratigraphic division of the SSG by comparing our interpreted fluvial planforms, bed grain size and paleohydraulic parameters *H* and *S* to similar modern rivers with known *W/H* ratios. The accuracy of *W* is further tested with reference to generalised, globally derived scaling relationships relating *W* and *H* (Galeazzi et al., 2021; Long et al., 2021; Greenberg et al., 2021).

The first method to constrain planform was an evaluation of the bar-dune angular difference (Δ_{db}, °) recorded by fluvial stratigraphy. This parameter discriminates between single-threaded and multi-threaded rivers (Valenza et al., 2026; McLeod et al., 2025), as multi-threaded rivers are generally dominated by downstream accreting bars, while lateral accretion is prevalent in single-threaded river systems (Miall, 1994; 2006). Bar-dune angular difference is calculated for each bar accretion package as the angle between the mean bar accretion direction relative to dune paleoflows. For each stratigraphic division, bars are classified as downstream accreting (Δ_{db}<45°), laterally accreting (45<Δ_{db}<135°) or upstream accreting (135<Δ_{db}<180°). Units mainly comprised of downstream accreting bars represent the deposits of low-sinuosity, multi-threaded rivers. Units mainly comprised of laterally accreting bars represent the deposits of high-sinuosity, meandering rivers.

Low-sinuosity, multi-threaded rivers encompass both anastomosing and braided planforms (Nanson and Knighton, 1996; Lyster et al., 2022). These two planforms are morphodynamically distinct, and distinguishing them is important for creating accurate depositional models and evaluating the response of rivers to external forcings, such as climate and tectonics (e.g. Galeazzi, 2021; Lyster et al., 2022 Wood et al., 2025; Mcleod et al., 2025). Hence, our interpretations of fluvial planform were further refined using observations of facies-scale and architectural-element scale sedimentology, allowing us to identify braided, anastomosing and meandering rivers. We recognise that planform definitions are inconsistent for anastomosing rivers (e.g. Nanson and Knighton, 1996; Makaske, 2001; Carling et al., 2014). We identify anastomosing rivers using the discriminator of Lyster et al. (2022), in which they are defined as multi-threaded rivers with stable bars.

To derive *W/H* for each stratigraphic division, the rivers of the HSF are compared to a database of sand bed modern rivers in the Kati Thanda-Lake Eyre Basin, Australia, as these modern systems are argued to be sedimentologically and climatically analogous to the SSG and time-equivalent deposits across NW Europe (Brookfield, 2008; McKie, 2014; Morón et al., 2014; English et al., 2024). For the CHF, we compare our results to the global modern dataset of Lyster et al. (2022), in the absence of recognised direct analogues. By identifying a suite of modern rivers with a comparable bed grain size, planform, *H* and *S*, we can extract geologically plausible values of *W/H* for the rivers of the SSG.

Where possible, we reference our resulting values of *W/H* to the globally generalised, combined scaling relations of Long (2021) and Galeazzi et al. (2021), and the scaling relation of Greenberg et al. (2022), applied to fully preserved laterally accreting bar surfaces. These scaling relations are detailed in **Supplementary Material 1**.

3.4. Unit and bankfull water discharge and sediment flux

Firstly, flow velocity (*U*, m/s) was calculated using the equation of Manning et al. (1890) (**Equation 4**). *U* is a function of *H*, *S,* and the roughness coefficient *n* (Lyster et al., 2021; Wood et al., 2022; Sharma et al., 2023; McLeod et al., 2025), commonly set as 0.03 based on the work of Chow (1959). Although *n* in natural channels can vary to some extent (Chow, 1959), *n* = 0.03 is appropriate both for gravel-bed rivers and sand-bed rivers with abundant dunes, and as uncertainty in *n* is small compared to other uncertainties in the palaeohydrological workflow, the use of a constant *n* does not substantially influence our results. Unit water discharge ($Q_{w,\,u}$, m²/s), water discharge per unit width, can then be calculated by multiplying *U* by *H* (**Equation 5**).

$$U = \frac{1}{n} H^{1.5} S^{0.5} \quad \textbf{(4)}$$

$$Q_{w,u} = UH \quad \textbf{(5)}$$

Bankfull water discharge ($Q_{w,bf}$, m³/s) is calculated by multiplying unit water discharge ($Q_{w,\,u}$) by W.

Bankfull sediment flux, ($Q_{w,bf}$, kg/s), is calculated from W and unit sediment flux ($Q_{s,\,u}$, kg/m/s). Although there are numerous methods for calculating $Q_{s,\,u}$ (e.g. Barry et al., 2004; Jacobs, 2022; Martin-Moreta et al., 2023), we use the method of Meyer-Peter and Müller (1948), modified by Wong and Parker (2006) to calculate bedload transport, and the method of Engelund and Hansen (1967) for suspended bedload transport. These methods are appropriate because they incorporate our paleohydraulic parameters without additional inputs, and have been used effectively to calculate sediment flux in the geological past by Sharma et al. (2023) and McLeod et al. (2025).

The method of Meyer-Peter and Müller (1948), modified by Wong and Parker (2006) gives $Q_{s,\,u}$ for bedload transport as:

$$Q_{s,u} = \rho_s \left(g{D_{50}}^3 \Delta\rho\right)^{0.5} C(\tau_{*b} - \tau_{*c})^{\alpha} \quad \textbf{(6)}$$

In **Equation 6**, ρ_s is the density of sediment, 2600 kg/m³, g is gravitational acceleration, 9.81m/s², and $\Delta\rho$ is the dimensionless submerged specific gravity of sediment, 1.6. Constants C and α are 4.93 and 1.6 respectively. τ_{*c} is the dimensionless critical shear stress, given as a range between 0.03 and 0.06, reflecting measurements taken from modern gravel-bed rivers (Peitit et al., 2015). τ_{*c} is the dimensionless bed shear stress, and is given as:

$$\tau_{*b} = \frac{HS}{\Delta\rho D_{50}} \quad \textbf{(7)}$$

The method of Engelund and Hansen (1967) gives $Q_{s,\,u}$ for the suspended part of the bedload as:

$$Q_{s,u} = \rho_s \left(g{D_{50}}^3 \Delta\rho\right)^{0.5} q_{*t} \quad \textbf{(8)}$$

In **Equation 8**, q_{*t} is the dimensionless Einstein number, which relates shear stress and bed friction. For an extended methodology, see **Supplementary Material 1**. For sand bed rivers, we calculate sediment flux using **Equation 6**. For gravel-bed rivers, we calculate sediment flux by summing the results of **Equation 6** and **Equation 8**.

4. Results

4.1. Sedimentology and sedimentary architecture

Studies of the SSG (Smith, 1990; Smith and Edwards, 1991; McKie and Williams, 2009; Newell, 2017b), have documented facies associations and sedimentary architecture of these deposits in some detail. We do not repeat this work here: instead we concentrate on key sedimentary observations that we contextualise with respect to our quantiative paleohydrological analyses.

In the outcrops studied, the upper and lower CHF are both composed of horizontally and vertically amalgamated, channelised conglomeratic bodies (**figs. 4a-d**). Texturally, conglomerates are structureless or imbricated. (**fig. 4e-f, 6a**). Clasts are dominantly rounded to well-rounded, are composed mainly of quartzite, and are of pebble to cobble grade in a matrix of coarse-grained sandstone (**fig. 4e-f, 6a)**. Two scales of hierarchically arranged inclined strata are observed. The smaller scale of cross-strata are between 3 and 10 cm thick, and are interpreted as dune deposits. Dune cross-stratification is comparatively rare due to the coarse grain size. Where present, dune deposits are arranged within thicker, shallowly inclined to subhorizontal cosets, 0.5-4.0 m thick, bounded by more laterally extensive boundaries; these are interpreted as bar deposits (**fig. 4a-d**). Bar deposits are either structureless, or show well-developed bar-scale stratification, with each bar set showing normal grading. The CHF also contains a subset of sandy barforms, with grain sizes between fine- and coarse-grained sandstone, and containing stringers and lag deposits of small pebbles (**figs. 4a-d)**. The sedimentary architecture of the lower and upper CHF are notably different. Conglomeratic barforms in the lower CHF are laterally extensive (>30 m), with steeply inclined bar accretion surfaces and channel cuts suggesting deep, confined channels (**fig. 4a, b**). In contrast, bars in the upper CHF are thinner, channel cuts are shallower in angle and depth, and sandstone facies are more common (**fig. 4c, d**). Clast size distributions are similar for the lower and upper CHF. Both units have a D_{50} of 40 mm. The lower CHF has a

D_{16} and D_{84} of 19 mm and 85 mm respectively, whereas the upper CHF has a D_{16} of 20 mm, and a D_{84} of 95 mm.

The HSF is mainly composed of laterally and vertically amalgamated sandstone bodies (**fig. 5a-d)**. Each sandstone body generally fines upwards from 0.05-0.2 m thick basal gravel lags into medium-grained sandstones 0.3-3.9 m thick, which are locally capped by mudstone-dominated strata (**fig. 5c, d**). Conglomerates are dominantly granule- and pebble-grade, and are cross-stratified. Conglomerates are composed of intraclasts of rhizocretions and mudstone, and extraclasts of vein quartz, quartzite and fine-grained volcanics. Sandstones frequently show two hierarchical scales of cross-stratification. Smaller-scale cross-sets are interpreted as dune deposits, and are 0.03-0.12 m thick. Dune cross-sets are arranged in shallowly inclined to subhorizontal bar-scale cosets, 0.3-3.9 m thick, bounded by more laterally extensive channelised boundaries (**fig. 5a-d)**. The Otterton Ledge Member is composed of simple sheet-like amalgamated channels with typical architectures as described above (**fig. 5a, b**). The Chiselbury Bay Member is composed of amalgamated channel sandstones with thicker, wider, and more architecturally diverse barforms. For example, bars often show well developed, convex lower bounding surfaces >5 m wide, with 1.5-4 m of erosional relief, which are interpreted as channel cuts (**fig. 5c, d**). Bars with gently dipping bounding surfaces and inclined, large-scale cosets oriented perpendicular to dune-scale cross-bedding are interpreted as laterally accreting bar packages. In the Pennington Point Member, isolated, laterally accreting sandstone bodies, showing the typified fining-upward succession, are encased within structureless to laminated mudstone and heterolithic strata, which are interpreted as overbank facies associations (**fig. 5e, f**). Throughout the HSF, the upper parts of barform-accretion and channel-fill elements are commonly overprinted by horizons of subvertical pedogenic rhizocretions: calcite nodules precipitated by phreatophytic vegetation (**fig. 6c, d**). Reworked rhizocretions also occur in lag deposits at the base of channelised bodies (**fig. 6e, f**). They are found in all three studied units; however they are most extensive in the Otterton Ledge Member (**fig. 6c**). *In situ* rhizocretions have maximum lengths of 1-2 m (**fig. 6c**), but are recorded to reach several metres (Purvis and Wright, 1991). Overall, sedimentological and architectural observations are consistent with those of previously published studies (Purvis and Wright, 1991; Lorsong and Atkinson, 1995; Svendsen and Hartley, 2001; Hounslow and McIntosh, 2003; Newell, 2017b).

In the SSG, dune paleoflow data record north- and northeast-directed paleocurrents (**Supplementary Material 1**). These measurements build on previously collected paleocurrent data (Sellwood et al., 1984; Smith and Edwards, 1991; Benton et al., 1993; Lorsong and Atkinson, 1995; Newell, 2017b), but increase the volume of data reported for the CHF by a factor of >8 (Smith and Edwards, 1991; **Supplementary Material 1**), and increase the spatial range of data in the HSF (Newell, 2017b). The collection of new paleocurrent data also allows dune paleoflows to be linked with bar accretion direction, in order to appraise Δ_{db}, a key parameter for inferring river planform.

4.2. Bankfull flow depths

From our dune-scale cross-set distributions (**Section 4.1**), the relationship between maximum cross-set height and mean height in the SSG is linear with a coefficient of 0.6 and a coefficient of determination (r^2) of 0.962 (**fig. 7a**). This relationship compares well with the results of previous studies (Lyster et al., 2021; Wood et al., 2022; Mcleod et al., 2025), suggesting that our cross-set scaling method is reliable. A Cumulative Distribution Function of reconstructed mean cross-set heights for the CHF is presented in **Figure 7b**. Median reconstructed cross set heights are 0.066 m for the lower CHF, and 0.072 m for the upper CHF (n = 23 and 25 respectively, **fig. 7b**). In the HSF, median cross set heights are 0.060 m for the Otterton Ledge Member, 0.075 m for the Chiselbury Bay Member, and 0.089 m for the Pennington Point Member (n = 114, 156 and 110 respectively, **fig. 7c**). These values imply that, for a bedform preservation ratio of 0.34 ± 0.067 (Leclair and Bridge, 2001), subaqueous dunes on the base of rivers had median heights of 0.19 ± 0.05 m in the lower CHF, and median heights of 0.21 ± 0.05 m in the upper CHF (**fig. 7b**). In the HSF, subaqueous dunes had median heights of 0.17 ± 0.04 m in the Otterton Ledge Member, 0.22 ± 0.05 m in the Chiselbury Bay Member, and 0.26 ± 0.06 m in the Pennington Point member (**fig. 7c**).

Bankfull flow depths (*H*) obtained using our bedform-based approach (**equations 1, 2**) range between 0.5 and 4.0 m (**fig. 8**). Significantly, for each stratigraphic division except the lower CHF, bedform-derived values of *H* are similar to values of *H* obtained from the thicknesses of bar-accretion architectural elements. This confirms that the two methods are generally compatible and that bedform- and barform-based approaches are consistent in their estimates of palaeo-flow depths (**fig. 8**). The dominantly conglomeratic lower CHF is an exception: *H* calculated from the bedform-based approach ranges between 0.8-2.8 m, whereas *H* calculated from the barform-based approach ranges between 2.1-4.6 m (**fig. 8**). This discrepancy is because, for coarse gravel bed rivers such as the CHF, flow conditions and grain size lie at the margins of the dune stability field (Dade and Friend, 1998). Consequently, dunes in the CHF are often absent and those observed are unlikely to record flow conditions in the largest channel threads.

Accordingly, for the lower CHF, values of *H* derived from the barform-based approach are propagated into the Monte Carlo workflow using a triangular distribution (n = 10^5) with a minimum of 2 m, a maximum of 6 m, and a mode of 2.5 m. For all other units, our statistically robust bedform-based results are propagated.

Bankfull flow depths (p_{10}, p_{90}) in the Olenekian-aged CHF are initially 2.4-4.8 m, with a median of 3.4 m (**fig. 9a**). Flow depths decrease to 1.2-2.0 m with a median of 1.7 m in the upper half of the unit. In the Anisian-Ladinian aged HSF (246.5-236.9 Ma, Yan et al., 2026), flow depths appear to increase over time. For the Otterton Ledge Member, which represents much of the temporal range of the HSF (246.5-241.2 Ma, **fig. 9a**), estimated flow depths are 1.0-2.0 m, with a median of 1.4 m. In the Chiselbury Bay Member (241.2-240.2 Ma), bankfull flow depths then increase to 1.2-2.5 m, with a median of 1.8 m. In the Pennington Point Member, reconstructed flow depths are 1.4-3.0 m, with a median of 2.1 m (**fig. 9a**, 240.2 – 239.6 Ma).

4.3. Grain size and paleoslope

In the conglomeratic CHF, the D_{50} grain size of clasts is 40 mm for both intervals. Sandstones in the HSF are dominantly medium- and coarse-grained (**fig. 6b**), with granule and pebble-grade lag deposits locally observed (**fig. 6e, f**). Overall, median grain sizes are 0.43 mm for the Otterton Ledge Member, 0.35 mm for the Chiselbury Bay Member, and 0.34 mm for the Pennington Point Member.

Calculated paleoslopes (S) are a function of bankfull flow depths (**fig. 9a**) and d_{50} grain size (**Equation 3,** Trampush et al., 2011). In the CHF, the median paleoslope was initially 1.0 $\times 10^{-3}$ m/m (i.e. 0.1%), and doubled to 2.0 $\times 10^{-3}$ m/m in the upper half of the unit (**fig. 9b**). In contrast, in the HSF, median paleoslopes progressively decreased through time (**fig. 9b)**: slope was initially 7.8 $\times 10^{-4}$ m/m in the Otterton Ledge Member (246.5-241.2 Ma), then 5.8 $\times 10^{-4}$ m/m in the Chiselbury Bay Member (241.2-240.2 Ma), and finally 5.0 $\times 10^{-4}$ m/m (i.e. 0.05%) in the Pennington Point Member (240.2-239.6 Ma).

4.4. Fluvial planform

Fluvial planform is first inferred from the angular difference between bar accretion direction and dune migration direction (Δ_{db}). In the HSF, median values of Δ_{db} are 34° for the Otterton Ledge Member, 33° for the Chiselbury Bay Member, and 86° for the Pennington Point Member (**fig. 10a**). These values indicate the lower two studied units of the HSF likely represent low-sinuosity, multithreaded rivers, whereas the uppermost unit represents a high sinuosity, meandering river system. An increase in the interquartile range of Δ_{db} is observed, from 48° in the Otterton Ledge Member to 75° Chiselbury Bay Member (**fig. 10a**). This change suggests that channel sinuosity increased between these two units. The abundance of pedogenic rhizocretions in the HSF, which are formed by living plants, indicate that bars were highly vegetated and likely stable (**section 4.4, figs 6a-f**). Modern calcretes require a minimum of hundreds of years to form (Candy et al., 2005; Alonso-Zarza, 2018) and provide a quantitative estimate of the timescales of barform stability. These observations strongly indicate that the multithreaded, low sinuosity rivers of the Otterton Ledge and Chiselbury Bay Members were anastomosing, and that the Pennington Point Member represents meandering river deposits.

In the conglomeratic CHF, a paucity of observed dunes prevents a full statistical analysis of data. However, Δ_{db} ranges from 1-108° in the lower CHF, and 1-115° in the upper CHF (**fig. 10a**). The spread of values observed, including very low angular differences, strongly suggests that both downstream and lateral accreting bars are preserved, indicating that the rivers of the CHF were low sinuosity and multithreaded. Detailed sedimentological and architectural evidence presented by Smith (1990) and Smith and Edwards (1991) suggest that the lower CHF was deposited by wandering rivers, and so are most consistent with an anastomosing planform, whereas the architecture of the upper CHF matches well with the Donjek River in Canada (Smith, 1990; Smith and Edwards, 1991), an exemplar braided river (Miall, 2006).

4.5. Total active channel width

For each stratigraphic division of the SSG, interpreted planform (braided, anastomosing, meandering), bed grain size (sand, gavel), bankfull flow depth (H) and slope (S) were compared with modern rivers to find appropriate analogues. Values of W/H recorded for these modern rivers can be used to estimate total active bankfull channel width (W) for the SSG.

Rivers of the CHF are compared against the global modern dataset of Lyster et al. (2022). For the lower CHF, the most similar modern gravel-bed rivers are between 1.6 and 6.8 m deep, and have slopes of 0.00035 - 0.0012 m/m (**fig. 11a**). For the upper CHF, similar gravel-bed rivers are between 0.52 and 1.9 m deep, and have slopes of 0.0015 - 0.0046 m/m (**fig. 11b**).

For the anastomosing Otterton Ledge and Chiselbury Bay members, comparable transects of the Marshall and Diamantina Rivers (Tooth and Nanson, 2004; Brunner, 2013; Nanson and Huang, 2017) contain reaches with median bankfull depths of 0.64-2.6 m, and slopes of 0.0013 and 0.00020 m/m (**fig. 11c, d**). For the meandering Pennington Point Member, comparable reaches of the Diamantina River have bankfull depths of 4.1-4.2 m, and slopes of 0.00020 m/m (**fig. 11e**).

From these modern river analogues, *W/H* ratios were obtained. For the lower CHF, comparable gravel-bed anastomosing rivers have a median *W/H* of 97. For the upper CHF, comparable gravel-bed braided rivers have a median *W/H* of 217 (**fig. 12**). For the Otterton Ledge and Chiselbury Bay members of the HSF, the median *W/H* of comparable sand-bed anastomosing rivers is 223 (**fig. 12**). For the Pennington Point Member of the HSF, the median *W/H* of comparable sand-bed meandering rivers is 24 (**fig. 12**).

W/H results for gravel-bed anastomosing rivers, gravel-bed braided rivers, and sand-bed meandering rivers were validated by using the scaling relationships of Galeazzi et al. (2021) and Long (2021) (**Supplementary Material 1**). This method produces a median *W/H* value of 76 for the lower CHF, 203 for the upper CHF, and 24 for the Pennington Point Member of the HSF (**fig. 12**), consistent with the results above. For sand-bed meandering rivers of the Pennington Point Member, values of *W/H* derived by the architecturally-based scaling relationship of Greenberg et al. (2021) (**Supplementary Material 1**) also fall within the range of values observed in comparable modern systems (**fig. 12**). Furthermore, interpreted planforms and corresponding values of W/H for the SSG correspond well with the *W/H* planform stability criterion taken from the global modern dataset of Lyster et al. (2022), which discriminates between single and multi-threaded rivers (**fig. 12**).

In summary, all methods of estimation suggest that median *W/H* ratios derived from comparable modern rivers for the SSG are geologically realistic. When combined with our results for *H* for the SSG, these *W/H* values can be confidently used to estimate *W*. Median values of *W* in the lower and upper Chester Formation are 330 m and 370 m, respectively. For the HSF, median *W* is 320 m in the Otterton Ledge Member, 400 m in the Chiselbury Bay Member, and 50 m in the Pennington Point Member (**Supplementary Material 1**).

4.6. Water and sediment discharge

Median unit water discharge ($Q_{w,\,u}$) is estimated at 7.8 m²/s for the lower CHF, and 3.7 m²/s for the upper CHF (**fig. 13a**). In the HSF, $Q_{w,\,u}$ increased over time. Median $Q_{w,\,u}$ was initially 1.8 m²/s in the Otterton Ledge Member (246.5-241.2 Ma), increasing to 2.1 m²/s in the Chiselbury Bay Member (241.2-240.2 Ma), and further increasing to 2.6 m²/s in the Pennington Point Member (240.2-239.6 Ma, **fig. 13a**).

Bankfull water discharges ($Q_{w,\,bf}$) are calculated from $Q_{w,\,u}$ and *W*. Overall, median values of $Q_{w,\,bf}$ are substantially higher for the CHF than the HSF. Median $Q_{w,\,bf}$ was 760 m³/s in the lower CHF, and 810 m³/s for the upper CHF (**fig. 14a**). In the HSF, median $Q_{w,\,bf}$ was 380 m³/s for the Otterton Ledge Member (246.5-241.2 Ma), and 480 m³/s for the Chiselbury Bay Member (241.2-240.2 Ma). $Q_{w,\,bf}$ was substantially lower in the Pennington Point Member, at 64 m³/s (240.2-239.6 Ma, **fig. 14a**).

Unit sediment fluxes ($Q_{s,\,u}$) are consistent throughout the SSG. Median values of $Q_{s,\,u}$ in the conglomeratic CHF are 11.9 kg/m/s for the lower part of the unit, and 12.1 kg/m/s for the upper part of the unit (**fig. 14a**). In the HSF, a median $Q_{s,\,u}$, of 11.5 kg/m/s is recovered for the Otterton Ledge Member, and a median $Q_{s,\,u}$ of 11.7 kg/m/s is recovered for both the Chiselbury Bay and Pennington Point Members (**fig. 14a**).

Bankfull sediment fluxes ($Q_{s,\,bf}$) are calculated from $Q_{s,\,u}$ and *W*. Median values of $Q_{s,\,bf}$ are 3940 kg/s for the lower CHF and 4530 kg/s for the upper CHF (**fig. 14b**). Median values of $Q_{s,\,bf}$ are 3670 kg/s for the Otterton Ledge Member (246.5 - 241.2 Ma), and 4670 kg/s for the Chiselbury Bay Member (241.2-240.2 Ma, **fig. 14b**). $Q_{w,\,bf}$ is substantially lower for the Pennington Point Member, at 603 kg/s (240.2-239.6 Ma, **fig. 14b**).

5. Discussion

5.1. Changing fluvial character in the Lower and Middle Triassic

Through our paleohydraulic workflow, we quantitatively reconstruct changing values of bankfull flow depth, slope, planform and water and sediment discharge for the SSG over time (**fig. 15**). Overall, the SSG can be divided between the gravel-bed CHF, and the sand-bed HSF.

Rivers in the lower CHF had median bankfull flow depths of 3.4 m and slopes of 1.0×10^{-3} m/m. These rivers likely had an anastomosing planform, with bankfull water discharges of ca. 760 m^3/s and sediment fluxes of up to 4000 kg/s (**fig. 15**). The rivers which deposited the upper CHF had median bankfull flow depths of 1.7 m and slopes of 2.0×10^{-3} m/m. These systems were likely braided, with bankfull water discharges of ca. 800 m^3/s and bankfull sediment fluxes of 4530 kg/s (**fig. 15**). Previous assessments of flow depth, derived from architectural observations, suggest that bankfull depths were 2-6 m in the CHF (Smith, 1990; Smith and Edwards, 1991), consistent with our quantitative paleohydraulic results (**fig. 9a**). Our results further show that the CHF, which had previously been considered a single lithostratigraphic unit, is best considered as having been deposited by two distinct types of river with differing sedimentary architecture, bankfull flow depths, paleoslopes and planforms. However, both have a similar gravel grain-size distribution (**section 4.1**) and comparable bankfull water and sediment discharges (**fig. 14b; 15b**), suggesting that rivers had similar hydraulic conditions. The similarity of grain size and bankfull discharge, but difference in paleoslope and planform suggests the change in fluvial style between the lower and upper CHF may have had a tectonic origin. However a climatic origin, such as a change in bankfull discharge frequency, cannot be excluded. This peturbation is likely recorded downstream of the Wessex Basin: a regional bipartite division of the CHF is also observed in the Worcester Graben and the Midlands Basins, 200-300 km north of the Wessex Basin (**fig. 1c,** Newell, 2017a).

In the HSF, the Otterton Ledge Member record rivers with a median bankfull flow depth of 1.4 m and slopes of 7.8 × 10^{-4} m/m. These rivers had an anastomosing planform, with bankfull water discharges of 380 m^3/s and sediment fluxes of up to 3670 kg/s (**fig. 15**). The rivers of the Chiselbury Bay Member had median depths of 1.8 m, slopes of 5.8 × 10^{-4} m/m. These rivers were also anastomosing, had bankfull water discharges of 480 m^3/s, and bankfull sediment fluxes of 4670 kg/s (**fig. 15**). The rivers of the Pennington Point Member had median depths of 2.1 m and slopes of 5.0 × 10^{-4} m/m. These rivers were meandering, with water discharges of ca. 645 m^3/s, and sediment fluxes of ca. 600 kg/s (**fig. 15**). For the Chiselbury Bay Member of the HSF, Lorsong and Atkinson (1995), and McKie and Williams (2009) estimated bankfull flow depths from facies and architectural observations, yielding values of 4-5 m and 3 m respectively. Our estimates of bankfull flow depth for this member range between 1.2 and 2.5 m (p_{10} and p_{90} respectively, **fig. 8**), which we systematically reconstruct from both bedform and architectural-scale measurements. We thus highlight the value of using quantitative approaches in accurately reconstructing channel hydraulics (Wood et al., 2025).

Within the HSF, a general proximal-distal transition is observed, with rivers showing decreasing grain size, decreasing slope and increasing sinuosity from base to top of the formation (**section 4.3; figs. 9b, 10**). These trends illustrate the shortening of the Sherwood-2 River System in response to the Muschelkalk transgression and coincident aridification (Bourquin et al., 2011; McKie, 2017; Newell, 2017a; Yan et al., 2026). Our results further suggest that rivers in the Chiselbury Bay Member records a brief (c. 1 Ma) time interval when rivers were deeper, more sinuous and had greater bankfull discharges than the rivers in the Otterton Ledge Member. A decrease in the abundance and size of pedogenic rhizocretions in the Chiselbury Bay Member may indicate a higher water table and increased precipitation. These interpretations are consistent with the depositional model of Newell (2017b), which suggested that this unit represented a brief humid period during the middle Triassic. Finally, the rivers of the Pennington Point Member record an abrupt eightfold decrease in bankfull water discharge and sediment flux (**fig. 15**). These rivers, which we interpret as meandering in line with previous architectural interpretations (Lorsong and Atkinson, 1995; Svendsen and Hartley, 2001; Newell and Shariatipour, 2016), likely record the distal segment of the fluvial system. The decreases in bankfull water discharge and sediment flux observed likely originate from the transmission loss of water, and the division of the trunk system into several active distributary branches (**fig. 15, 16c,** Lang et al., 2004) where the Helsby Sandstone fluvial system discharged into the playa lake facies represented by the Mercia Mudstone Group (Howard et al., 2008).

Significantly, our paleohydraulic and sedimentological observations suggest that the HSF is temporally dominated by anastomosing rivers (**fig. 15**). This contrasts with previous interpretations of these units as braided river deposits (Sellwood et al., 1984; Purvis and Wright, 1991; Lorsong and Atkinson, 1995; Newell, 2017b; Coram et al., 2019). Although our paleohydraulic data confirm that rivers in the Otterton Ledge and Chiselbury Bay Members were low-sinuosity and multithreaded, the abundance of pedogenic rhizocretions suggests that these rivers had vegetated, stable bars (**Section. 4.4, fig. 15**). Estimated values of flow depth, slope, grain size and planform further suggest that these rivers are comparable to modern dryland anastomosing rivers in Australia (**figs. 11c-e, 16a, b**). These systems are sedimentologically and morphodynamically different from their humid counterparts (Nanson and Knighton, 1996; North et al., 2007). Humid zone anastomosing rivers comprise isolated sandstone channel-fill bodies encased within fine-grained floodplain deposits (Nanson and Knighton, 1996; North et al., 2007; Wood et al., 2022; McLeod et al., 2025). In contrast, dryland anastomosing rivers are sand-dominated, contain complex anabranches and have wide channel belts (**fig. 16a, b,** Tooth and Nanson, 1999; Lang et al., 2004; North et al., 2007). These attributes appear consistent with our observations of the Otterton Ledge and Chiselbury Bay Members, indicating that the HSF records a compelling example of dryland anastomosing rivers in the geological record.

5.2. Climate as a driver of river behaviour in the Sherwood Sandstone Group

Both the CHF and HSF were deposited in a climatically and tectonically dynamic setting (e.g. Bourquin et al., 2011; Radley and Coram, 2016; Newell, 2017a; b; Yan et al., 2026). In particular, the CHF is notable for its widespread distribution of conglomeratic facies (Radley and Coram, 2016). Conglomeratic facies persist into the British Midlands c. 300 km north of the Devon coastal section, and c. 400 km north of their source area (**fig. 1c,** e.g. Buist and Thompson, 1982; Steel and Thompson, 1983; Rees and Wilson, 1998). In contrast, similar source-to-sink systems draining from the Variscan mountains during the mid-Triassic and upper Carboniferous are sand bedded throughout (Hallsworth et al., 2000; Wood et al., 2022; Yan et al., 2026). Any sediment sourcing control on the coarse grain size of this unit is unlikely: the well-rounded, dominantly quartzite clasts abundant in the CHF likely originate from the Gallic Massif in north France (**fig. 1a**; Plant et al., 1999; Sendino, 2012; Radley and Coram, 2015) rather than more proximal, local sources, where the pre-Triassic basement is largely sedimentary (**fig. 1c**, Yan et al., 2026).

The magnitude of hydrological change between the CHF and the HSF becomes apparent when our paleohydraulic results are combined with catchment reconstructions and paleoclimate constraints. Quantitative provenance analysis suggests that drainage length scales doubled to quadrupled between the CHF and HSF, from c. 100 km to 200-400 km (Morton et al., 2013), corresponding with a regional drainage organisation triggered by the Hardegsen tectonic event (e.g. Bourquin et al., 2011; von Eynatten et al., 2026). Using the geomorphic scaling relation of Nyberg et al. (2018), catchment areas are inferred to be c. 1600 km² for the CHF, and 5800 – 20,000 km² for the HSF: increasing by a factor between 4 and 12. These contrast with our paleohydraulic results, which show that bankfull water discharges in the CHF were double those of the HSF, and that sediment fluxes were comparable for both units. Effective daily precipitation, calculated from the bankfull water discharges and the catchment areas of these systems, are c. 40 mm/day in the CHF, and ca. 2-6 mm/day in the HSF, suggesting that precipitation driving these discharge events was 7 to 20 times more intense in the early Triassic than the middle Triassic. However, the climate was semiarid for both intervals: long-term runoffs of approximately 130 mm/y are reconstructed for the early Triassic (Ravida et al., 2021), and 100-250 mm/y for the middle Triassic, inferred from the presence of calcretes (**fig. 6c-f,** Eide et al., 2018). These findings suggest that bankfull discharge events in the lower Triassic CHF were generated by intense but infrequent precipitation events which mobilised large amounts of gravel grade material.

Climate change affects both the hydraulic regime of fluvial systems and the grain size of exported sediment (e.g. Armitage et al., 2011; McLeod et al., 2024). Hyperthermal events in particular are associated with widespread landscape devegetation, bedrock erosion and changes in preciptiation regime. Rapid global warming of 5 °C over c. 270 kyr (Inglis et al., 2020; Piedrahita et al., 2025) during the Paleocene-Eocene Thermal Maximum is well documented to have produced a coarsening of fluvial grain size, as well as extreme bankfull discharges from an intensified precipitation (e.g. Schmitz and Pujalte, 2007; Foreman et al., 2012; Carmichael et al., 2017; Van Praagh et al., 2024; Prieur et al., 2025; Willard et al., 2026). Accordingly, we suggest the sedimentological and paleohydraulic character of the CHF is indicative of an analogous lower Triassic hyperthermal. Based on regional stratigraphic correlation, the CHF is suggested to be of Smithian Age in the Olenekian Stage (Bourquin et al., 2011). This interval coincides with the Late Smithian Thermal Maximum (LSTM, Sun et al., 2012; Lindström et al., 2019; Du et al., 2022; Armores et al., 2025). The LSTM was a c. 0.5 My-long hyperthermal triggered by activity from the Siberian Large Igneous Province (Du et al., 2022), where terrestrial temperatures, already elevated in the early Triassic, reached 35-40°C (Sun et al., 2012). These extreme conditions triggered mass landscape devegetation at low latitudes (Sun et al., 2012; Linström et al., 2019) and caused severe perturbations in the global hydrological cycle (Linström et al., 2019). These effects are consistent with the bedrock erosion required to generate the abnormally coarse grain size of the CHF, as well as the highly perturbed hydraulic regime observed. Infrequent but extreme rainfall is argued to have been generated by enhanced Tethyan monsoons passing north over the remnant Variscan mountain belt (**fig. 1a;** e.g. McKie, 2014; Ravida et al., 2021): monsoonal weather systems are known to be highly sensitive to climate change (Loo et al., 2015; Meijer et al., 2024). Although tectonic forcings can also change the grain size profile of rivers (e.g. Duller et al., 2010; Armitage et al., 2011; Whittaker et al., 2011; Hampson et al., 2014; Reynolds, 2024), it is unlikely that substantial tectonic activity contributed to the sedimentological-paleohydraulic changes observed in the CHF: paleoslopes for this unit (c. 1.0×10^{-3} m/m) are generally similar to the HSF (c. 7.8×10^{-4} m/m, **fig. 9b**), and to paleoslopes recovered for the Carboniferous rivers of the Variscan foreland (c. 4.5×10^{-4}, Wood et al., 2022).

Our findings provide empirical, quantitative evidence that the LSTM may have been the driver of the low frequency, high-discharge hydraulic regime previously proposed for the lower Triassic (e.g. Gallois, 2014; Radley and Coram, 2016; Newell, 2017a). More broadly, the LSTM represents an isolated, intense episode of fluvial activity within a generally arid lower Triassic interval (e.g. Bourquin et al., 2011; Newell, 2017b). Sustained fluvial activity was only later established during the mid-Triassic (**fig. 15**; e.g. Ambrose et al., 2014; Newell, 2017a; b), with rivers being sourced by regular precipitation under a relatively stable climate, evidenced by the abundance of vegetation **(section 4.4, 5.1)** and diverse biosphere (Benton et al., 2002; Dunhill et al., 2013; Coram et al., 2019).

Regionally, the CHF has multiple stratigraphic equivalents around northwest Europe (Bourquin et al., 2011). These deposits consist of stratigraphically confined, texturally and compositionally mature conglomerate sheets, often capped by a ventifact surface (e.g. Ramos and Sopena, 1989; Durand et al., 2006; Bourquin et al. 2006; 2007; Costamagna, 2012). The association of these deposits with the LSTM may not only provide a key stratigraphic constraint in the typically barren lower Triassic, but record the continental response to a global, early Triassic hyperthermal which has hitherto proved difficult to identify and correlate.

6. Conclusions

The lower-to-middle Triassic Sherwood Sandstone Group, UK, comprises the deposits of dryland river systems which serve as a reservoir unit crucial for the energy transition, and record landscape evolution during and after the Permo-Triassic extinction. Through quantitative paleohydrology and facies-based sedimentological observations of a complete section of the Sherwood Sandstone Group in Devon, southwest UK, we quantitatively reconstruct paleoslopes, planforms, bankfull water discharge and bankfull sediment fluxes for these ancient rivers. In the conglomeratic Chester Formation, rivers were firstly anastomosing and subsequently braided. Paleoslopes were c. 1.0-2.0 × 10^{-3} m/m, bankfull water discharges were 760-810 m^3/s, and bankfull sediment fluxes were 3940-4530 kg/s. For most of the Helsby Sandstone Formation (c. 246.5-240.6 Ma), rivers were anastomosing, and were active under a stable, semiarid climate, with clear evidence of paleosols and vegetated, stable bars. Bankfull water discharges were 380-480 m^3/s, and bankfull sediment fluxes were 3670-4670 m^3/s.

From the base to the top of the Helsby Sandstone Formation, a clear proximal-to-distal transition is observed. Paleoslope progressively decreases through time, from 7.8 × 10^{-4} m/m in the Otterton Ledge Member to 5.0 × 10^{-4} m/m in the Pennington Point Member, accompanied by an increase in channel sinuosity. Furthermore, the paleohydrology and sedimentology of the meandering Pennington Point Member, in which an abrupt, eightfold decrease in bankfull water discharge and bankfull sediment flux is observed, is consistent with depositional models for a terminal splay system. Overall, these proximal-to-distal paleohydraulic and sedimentological trends were most likely caused by the Muschelkalk marine transgression and synchronous regional aridification. The sedimentology, climate and paleohydrology of anastomosing and meandering rivers of the Helsby Sandstone Formation indicate that they were comparable with modern dryland rivers of the Kati Thanda-Lake Eyre Basin, Australia. These systems may serve as suitable depositional analogues for sand-bedded rivers in the Sherwood Sandstone Group.

When the paleohydrology of the Chester Formation and the Helsby Sandstone Formation are integrated with catchment and paleoclimate constraints, we show that precipitation during the lower Triassic was likely 7-20 times more intense than that in the mid-Triassic. However, long-term average precipitation remained comparatively constant throughout, implying that changes in the frequency and magnitude of extreme rainfall events may have influenced deposition in the lower Triassic CHF. The hydraulic characteristics and coarse grain size of this unit suggest a perturbed hydrological cycle and widespread landscape devegetation, and are consistent with the effects of hyperthermal climatic events. Existing stratigraphic constraints suggest the c. 0.5 Myr-long Late Smithian Thermal Maximum (c. 248 Ma) is a plausible driver behind the deposition of the Chester Formation, as well as equivalent units across NW Europe. We thus demonstrate the value of quantitative paleohydraulic methods, which use direct measurements of preserved fluvial stratigraphy, in reconstructing climate signals in a paleontologically barren, continental setting.

7. Acknowledgements

We thank Andy Newell for insightful discussions about the SSG in Devon, and Jonah McLeod for advice on applying quantitative paleohydrological methods. We thank Ladram Bay Holiday Park for granting us permission to access outcrops.

8. Funding statement

This work was funded by the Natural Environment Research Council (Grant NE/S007415/1).

9. Conflict of interest statement

The authors declare that they have no known competing financial interests or personal relationships that could have appeared to influence the work reported in this paper.

10. Data Availability Statement

Data available in article supplementary material

11. References

Alonso-Zarza, A.M., 2018. Study of a modern calcrete forming in Guadalajara, Central Spain: An analogue for ancient root calcretes. *Sedimentary Geology*, *373*, pp.180-190. https://doi.org/10.1016/j.sedgeo.2018.06.006

Ambrose, K., Hough, E., Smith, N. J. P., and Warrington, G., 2014. Lithostratigraphy of the Sherwood Sandstone Group of England, Wales and south-west Scotland. British Geological Survey Research Report, RR/14/01.

Amores, M., Frank, T.D., Fielding, C.R., Hren, M.T. and Mays, C., 2025. Age-controlled south polar floral trends show a staggered Early Triassic gymnosperm recovery following the end-Permian event. *Geological Society of America Bulletin*, *137*(7-8), pp.3255-3282. https://doi.org/10.1130/B38017.1

Benton, M.J. and Newell, A.J., 2014. Impacts of global warming on Permo-Triassic terrestrial ecosystems. *Gondwana Research*, *25*(4), pp.1308-1337. http://dx.doi.org/10.1016/j.gr.2012.12.010

Blum, M.D. and Törnqvist, T.E., 2000. Fluvial responses to climate and sea-level change: a review and look forward. *Sedimentology*, *47*, pp.2-48. https://doi.org/10.1046/j.1365-3091.2000.00008.x

Benton, M.J. and Spencer, P.S. 1995. British Triassic fossil reptile sites. In: Fossil Reptiles of Great Britain. Springer, Dordrecht, https://doi.org/10.1007/978-94-011-0519-4_4

Benton, M. J., Warrington, G., Newell, A. J., and Spencer, P. S. 1994. A review of the British Middle Triassic tetrapod assemblages. In Fraser, N. C. and Sues, H.-D. (eds), In the shadow of the dinosaurs, pp. 131-160. Cambridge University Press, Cambridge, 435 pp.

Bhattacharya, J.P., Copeland, P., Lawton, T.F. and Holbrook, J., 2016. Estimation of source area, river paleo-discharge, paleoslope, and sediment budgets of linked deep-time depositional systems and implications for hydrocarbon potential. *Earth-Science Reviews*, *153*, pp.77-110. https://doi.org/10.1016/j.earscirev.2015.10.013

Bourquin, S., Peron, S. and Durand, M., 2006. Lower Triassic sequence stratigraphy of the western part of the Germanic Basin (west of Black Forest): fluvial system evolution through time and space. *Sedimentary Geology*, *186*(3-4), pp.187-211. https://doi.org/10.1016/j.sedgeo.2005.11.018

Bourquin, S., Durand, M., Diez, J.B., Broutin, J. and Fluteau, F., 2007. The Permian-Triassic boundary and lower Triassic sedimentation in western European basins: an overview. *Journal of Iberian Geology*, *33*(2), pp.221-236. https://doi.org/10.5209/JIGE.33912

Bourquin, S., Bercovici, A., López-Gómez, J., Diez, J.B., Broutin, J., Ronchi, A., Durand, M., Arché, A., Linol, B. and Amour, F., 2011. The Permian–Triassic transition and the onset of Mesozoic sedimentation at the northwestern peri-Tethyan domain scale: palaeogeographic maps and geodynamic implications. *Palaeogeography, Palaeoclimatology, Palaeoecology*, *299*(1-2), pp.265-280. https://doi.org/10.1016/j.palaeo.2010.11.007

Bradley, R.W. and Venditti, J.G., 2017. Reevaluating dune scaling relations. *Earth-science reviews*, *165*, pp.356-376. http://dx.doi.org/10.1016/j.earscirev.2016.11.004

Breeze, D., Scarselli, N., Hampson, G.J. and Chiarella, D., 2026. A review of multi-scale sedimentological heterogeneities in the Ormskirk Sandstone Formation of the East Irish Sea Basin and their impact on the injection and migration of CO2. *Journal of the Geological Society*, *183*(3), pp.jgs2025-099. https://doi.org/10.1144/jgs2025-099

Brémaud, M., Burnside, N.M., Shipton, Z.K., Bossennec, C., Fuchs, S. and Deon, F., 2026. How useful are outcrop samples to constrain subsurface thermal properties for geothermal exploration? Case study from the Chester formation, UK. *Geothermics*, *136*, p.103617. https://doi.org/10.1016/j.geothermics.2026.103617

Brookfield, M.E., 2008. Palaeoenvironments and palaeotectonics of the arid to hyperarid intracontinental latest Permian-late Triassic Solway basin (UK). *Sedimentary Geology*, *210*(1-2), pp.27-47. https://doi.org/10.1016/j.sedgeo.2008.06.003

Brunner, P.R., 2013. Dryland Channel Forms and Processes: A Whole Catchment Scale Study of the Diamantina River, Central Australia. https://dx.doi.org/10.25904/1912/1345

Buist, D.S. and Thompson, D.B., 1982) Sedimentology, engineering properties and exploitation of pebble beds in the Sherwood Sandstone Group (Lower Trias) of North Staffordshire with particular reference to highway schemes. Mercian Geologist, 8, 241-269.

Burgess, P.M., Dobromylskyj, E. and Lovell–Kennedy, J., 2025. Probably proximal pebbles? An outcrop-constrained quantitative analysis of clast transport distances in the lower Triassic Sherwood Sandstone Group, UK. *Journal of the Geological Society*, *182*(3), pp.jgs2024-155. https://doi.org/10.1144/jgs2024-155

Burley, S.D., 1987. *Diagenetic modelling in the Triassic Sherwood sandstone group of England and its offshore equivalents, United Kingdom continental shelf* (Doctoral dissertation, University of Hull).

Candy, I., Black, S. and Sellwood, B.W., 2005. U-series isochron dating of immature and mature calcretes as a basis for constructing Quaternary landform chronologies for the Sorbas basin, southeast Spain. *Quaternary Research*, *64*(1), pp.100-111. https://doi.org/10.1016/j.yqres.2005.05.002

Carling, P., Jansen, J. and Meshkova, L., 2014. Multichannel rivers: their definition and classification. *Earth Surface processes and landforms*, *39*(1), pp.26-37. https://doi.org/10.1002/esp.3419

Carmichael, M.J., Inglis, G.N., Badger, M.P., Naafs, B.D.A., Behrooz, L., Remmelzwaal, S., Monteiro, F.M., Rohrssen, M., Farnsworth, A., Buss, H.L. and Dickson, A.J., 2017. Hydrological and associated biogeochemical consequences of rapid global warming during the Paleocene-Eocene Thermal Maximum. *Global and Planetary Change*, *157*, pp.114-138. http://dx.doi.org/10.1016/j.gloplacha.2017.07.014

Castelltort, S., Fillon, C., Lasseur, É, Ortiz, A., Robin, C., Guillocheau, F., Tremblin, M., Bessin, P., Guerit, L., Dekoninck, A., Allanic, C., Gautheron, C., Barbarand, J., Loget, N., Uzel, J., Yans, J., Briais, J., Al-Reda, M., Baby, G., François, T., Roig, J. & Calassou, S. (2023). The Source-to-Sink Vade-mecum: History, Concepts and Tools. Society for Sedimentary Geology. CSP 16. http://doi.org/10.2110/sepmcsp.16

Chedburn, L., Underhill, J.R., Head, S. and Jamieson, R., 2022. The critical evaluation of carbon dioxide subsurface storage sites: Geological challenges in the depleted fields of Liverpool Bay. *AAPG bulletin*, *106*(9), pp.1753-1789. https://doi.org/10.1306/07062221120

Chow, V.T. 1959. Open-Channel Hydraulics. McGraw–Hill, New York.

Colombera, L., Mountney, N.P. and McCaffrey, W.D., 2013. A quantitative approach to fluvial facies models: Methods and example results. *Sedimentology*, *60*(6), pp.1526-1558. https://doi.org/10.1111/sed.12050

Coram, R.A., Radley, J.D. and Benton, M.J.. 2019 The Middle Triassic (Anisian) Otter Sandstone biota (Devon, UK): review, recent discoveries and ways ahead. Proceedings of the Geologists' Association, 130, 294–306, https://doi.org/10.1016/j.pgeola.2017.06.007

Costamagna, L.G., 2012. Alluvial, aeolian and tidal deposits in the Lower to Middle Triassic" Buntsandstein" of NW Sardinia (Italy): a new interpretation of the Neo-Tethys transgression. *Zeitschrift der Deutschen Gesellschaft fur Geowissenschaften*, *163*(2), p.165. https://doi.org/10.1127/1860-1804/2012/0163-0165

Dade, W.B. and Friend, P.F., 1998. Grain-size, sediment-transport regime, and channel slope in alluvial rivers. *The journal of Geology*, *106*(6), pp.661-676. https://doi.org/10.1086/516052

Downing, R.A., Allen, D.J., Barker, J.A., Burgess, W.G., Gray, D.A., Price, M. and Smith, I.F., 1984. Geothermal exploration at Southampton in the UK: a case study of a low enthalpy resource. *Energy exploration and exploitation*, *2*(4), pp.327-342. https://doi.org/10.1177/014459878400200404

Du, Y., Song, H., Algeo, T.J., Song, H., Tian, L., Chu, D., Shi, W., Li, C. and Tong, J., 2022. A massive magmatic degassing event drove the Late Smithian Thermal Maximum and Smithian–Spathian boundary mass extinction. *Global and Planetary Change*, *215*, p.103878. https://doi.org/10.1016/j.gloplacha.2022.103878

Duller, R.A., Whittaker, A.C., Fedele, J.J., Whitchurch, A.L., Springett, J., Smithells, R., Fordyce, S. and Allen, P.A., 2010. From grain size to tectonics. *Journal of Geophysical Research: Earth Surface*, *115*(F3). http://dx.doi.org/10.1029/2009JF001495

Dunhill, A.M., Benton, M.J., Newell, A.J. and Twitchett, R.J., 2013. Completeness of the fossil record and the validity of sampling proxies: a case study from the Triassic of England and Wales. *Journal of the Geological Society*, *170*(2), pp.291-300. https://doi.org/10.1144/jgs2012-025

Durand, M., 2006. The problem of the transition from the Permian to the Triassic Series in southeastern France: comparison with other Peritethyan regions. Geological Society, London, Special Publications, 265, 281–296. https://doi.org/10.1144/GSL.SP.2006.265.01.13

Eide, C. H., Müller, R., Helland-Hansen, W. & Manville, V. (2018) Using climate to relate water discharge and area in modern and ancient catchments. *Sedimentology.* 65 (4), 1378-1389. https://doi.org/10.1111/sed.12426.

Engelund, F. and Hansen, E., 1967. A monograph on sediment transport in alluvial streams.

English, K.L., English, J.M., Moscardini, R., Haughton, P.D., Raine, R.J. and Cooper, M., 2024. Review of Triassic Sherwood Sandstone Group reservoirs of Ireland and Great Britain and their future role in geoenergy applications. *Geoenergy*, *2*(1), pp.geoenergy2023-042. https://doi.org/10.1144/geoenergy2023-042

von Eynatten, H., Sass, K., Dunkl, I. and Schönig, J., 2026. Extension and clockwise shift of central to western Europe's drainage across the Permo-Triassic transition. International Journal of Earth Sciences, 115(3), p.32. https://doi.org/10.1007/s00531-026-02574-x

Fielding, C.R., Alexander, J. and Allen, J.P., 2018. The role of discharge variability in the formation and preservation of alluvial sediment bodies. Sedimentary Geology, 365, pp.1-20. https://doi.org/10.1016/j.sedgeo.2017.12.022

Foreman, B.Z., Heller, P.L. and Clementz, M.T., 2012. Fluvial response to abrupt global warming at the Palaeocene/Eocene boundary. Nature, 491(7422), pp.92-95. https://doi.org/10.1038/nature11513

Franklin, J., Tyrrell, S., O'Sullivan, G., Nauton-Fourteu, M. and Raine, R., 2020. Provenance of Triassic sandstones in the basins of Northern Ireland—Implications for NW European Triassic palaeodrainage. *Geological Journal*, *55*(7), pp.5432-5450. https://doi.org/10.1002/gj.3697

Galeazzi, C.P., Almeida, R.P.D. and Do Prado, A.H., 2021. Linking rivers to the rock record: Channel patterns and paleocurrent circular variance. *Geology*, *49*(11), pp.1402-1407. https://doi.org/10.1130/G49121.1

Gallois, R.W., 2014. The position of the Permo-Triassic boundary in Devon, UK. Geoscience in South-West England, 13, pp.328-338.

Ganti, V., Whittaker, A.C., Lamb, M.P. and Fischer, W.W., 2019. Low-gradient, single-threaded rivers prior to greening of the continents. Proceedings of the National Academy of Sciences, 116(24), pp.11652-11657. https://www.pnas.org/cgi/doi/10.1073/pnas.1901642116

Gasanzade, F. and Bauer, S., 2025. Subsurface potential in the German North Sea sector for geological carbon dioxide storage: new insights on capacity assessment. Environmental earth sciences, 84(12), p.340. https://doi.org/10.1007/s12665-025-12351-9

Greenberg, E., Ganti, V. and Hajek, E., 2021. Quantifying bankfull flow width using preserved bar clinoforms from fluvial strata. Geology, 49(9), pp.1038-1043. https://doi.org/10.1130/G48729.1

Hallsworth, C.R., Morton, A.C., Claoué-Long, J. and Fanning, C.M., 2000. Carboniferous sand provenance in the Pennine Basin, UK: constraints from heavy mineral and detrital zircon age data. *Sedimentary Geology*, *137*(3-4), pp.147-185. https://doi.org/10.1016/S0037-0738(00)00153-6

Hampson, G.J., Duller, R.A., Petter, A.L., Robinson, R.A. and Allen, P.A., 2014. Mass-balance constraints on stratigraphic interpretation of linked alluvial–coastal–shelfal deposits from source to sink: example from Cretaceous Western Interior Basin, Utah and Colorado, USA. *Journal of Sedimentary Research*, *84*(11), pp.935-960. http://dx.doi.org/10.2110/jsr.2014.78

Henares, S., Donselaar, M.E. and Caracciolo, L., 2020. Depositional controls on sediment properties in dryland rivers: Influence on near-surface diagenesis. Earth-Science Reviews, 208, p.103297. https://doi.org/10.1016/j.earscirev.2020.103297

Hjelm, L., Anthonsen, K.L., Dideriksen, K., Nielsen, C.M., Nielsen, L.H. and Mathiesen, A., 2020. Evaluation of the CO2 storage potential in Denmark. *Danmarks og Grønlands Geologiske Undersøgelse Rapport*, *46*, p.2020.

Hossain, S., Hampson, G.J., Jacquemyn, C., Jackson, M.D. and Chiarella, D., 2024. Permeability characterisation of sedimentological facies in the Bunter Sandstone Formation, Endurance CO2 storage site, offshore UK. *International Journal of Greenhouse Gas Control*, *135*, p.104140. https://doi.org/10.1016/j.ijggc.2024.104140

Hounslow, M.W. and Gallois, R., 2023. Magnetostratigraphy of the Mercia Mudstone Group (Devon, UK): implications for regional relationships and chronostratigraphy in the Middle to Late Triassic of Western Europe. *Journal of the Geological Society*, *180*(4), pp.jgB2022-173. https://doi.org/10.1144/jgs2022-173

Hounslow, M.W., McIntosh, G., Edwards, R.A., Laming, D.J. and Karloukovski, V., 2017. End of the Kiaman Superchron in the Permian of SW England: magnetostratigraphy of the Aylesbeare Mudstone and Exeter groups. *Journal of the Geological Society*, *174*(1), pp.56-74. https://doi.org/10.1144/jgs2015-141

Hounslow, M.W. and McIntosh, G., 2003. Magnetostratigraphy of the Sherwood Sandstone Group (Lower and Middle Triassic), south Devon, UK: detailed correlation of the marine and non-marine Anisian. *Palaeogeography, Palaeoclimatology, Palaeoecology*, *193*(2), pp.325-348. https://doi.org/10.1016/S0031-0182(03)00235-9

Howard, A S, Warrington, G, Ambrose, K, and Rees, J G. 2008. A formational framework for the Mercia Mudstone Group (Triassic) of England and Wales. British Geological Survey Research Report, RR/08/04.

Inglis, G.N., Bragg, F., Burls, N.J., Cramwinckel, M.J., Evans, D., Foster, G.L., Huber, M., Lunt, D.J., Siler, N., Steinig, S. and Tierney, J.E., 2020. Global mean surface temperature and climate sensitivity of the early Eocene Climatic Optimum (EECO), Paleocene–Eocene Thermal Maximum (PETM), and latest Paleocene. *Climate of the Past*, *16*(5), pp.1953-1968. https://doi.org/10.1016/j.ijggc.2024.104140

Jones, C.M. and Collinson, J.D., 2025. Discussion on ‘Rivers of the Variscan Foreland: fluvial morphodynamics in the Pennant Formation of South Wales, UK’ by Wood et al. 2022 (JGS, 180, jgs2022-048). Journal of the Geological Society, 182(5), pp.jgs2025-033. https://doi.org/10.1144/jgs2025-033

Lang, S.C., Payenberg, T.H.D., Reilly, M.R.W., Hicks, T., Benson, J. and Kassan, J., 2004. Modern analogues for dryland sandy fluvial-lacustrine deltas and terminal splay reservoirs. *The APPEA Journal*, *44*(1), pp.329-356. https://doi.org/10.1071/AJ03012

Leclair, S.F. and Bridge, J.S., 2001. Quantitative interpretation of sedimentary structures formed by river dunes. Journal of Sedimentary Research, 71(5), pp.713-716. https://doi.org/10.1306/2DC40962-0E47-11D7-8643000102C1865D

Leonard, A.J., AG, M. and EB, S., 1982. Ventifacts from a deflation surface marking the top of the Budleigh Salterton Pebble Beds, east Devon. Proceedings of the Ussher Society 5, 333.

Lindström, S., Bjerager, M., Alsen, P., Sanei, H. and Bojesen-Koefoed, J., 2020. The Smithian–Spathian boundary in North Greenland: implications for extreme global climate changes. *Geological Magazine*, *157*(10), pp.1547-1567. https://doi.org/10.1017/S0016756819000669

Long, D.G., 2021. Trickling down the paleoslope: an empirical approach to paleohydrology. *Earth-Science Reviews*, *220*, p.103740. https://doi.org/10.1016/j.earscirev.2021.103740

Loo, Y.Y., Billa, L. and Singh, A. (2015) Effect of climate change on seasonal monsoon in Asia and its impact on the variability of monsoon rainfall in Southeast Asia. Geoscience Frontiers, 6, 817–823. https://doi.org/10.1016/j.gsf.2014.02.009

Lorsong, J.A. and Atkinson, C.D., 1995. Sedimentology and stratigraphy of Lower Triassic alluvial deposits, East Devon coast. *Excursion guide. Petroleum Group. Geological Society, London*.

Lyster, S.J., Whittaker, A.C., Hampson, G.J., Hajek, E.A., Allison, P.A. and Lathrop, B.A., 2021. Reconstructing the morphologies and hydrodynamics of ancient rivers from source to sink: Cretaceous Western Interior Basin, Utah, USA. Sedimentology, 68(6), pp.2854-2886. https://doi.org/10.1111/sed.12877

Lyster, S.J., Whittaker, A.C. and Hajek, E.A., 2022. The problem of paleo-planforms. *Geology*, *50*(7), pp.822-826. https://doi.org/10.1130/G49867.1

Makaske, B., 2001. Anastomosing rivers: a review of their classification, origin and sedimentary products. *Earth-Science Reviews*, *53*(3-4), pp.149-196. https://doi.org/10.1016/S0012-8252(00)00038-6

McLeod, J.S., Whittaker, A.C., Hampson, G.J., Bell, R.E., Prieur, M., Fuller-Field, O.G., Valero, L., Yan, X. and Valenza, J.M., 2025. Hothouse Hydrology: Evolving River Dynamics in the Eocene Montllobat and Castissent Formations, Southern Pyrenees. *Basin Research*, *37*(5), p.e70059. https://doi.org/10.1111/bre.70059

McLeod, J.S., Wood, J., Lyster, S.J., Valenza, J.M., Spencer, A.R. and Whittaker, A.C., 2023. Quantitative constraints on flood variability in the rock record. Nature Communications, 14(1), p.3362. https://doi.org/10.1038/s41467-023-38967-8

McKie, T., 2011. A comparison of modern Dryland depositional systems with the Rotliegend group in the Netherlands. SEPM Special Publications. 98. 89-103. https://doi.org/10.2110/pec.11.98.0089.

McKie, T., 2014. Climatic and tectonic controls on Triassic dryland terminal fluvial system architecture, central North Sea. In: Martinius, A.W., Ravnås, R., Howell, J.A., Steel, R.J. and Wonham, J.P. (eds) From Depositional Systems to Sedimentary Successions on the Norwegian Continental Shelf. Blackwell, Oxford, 46, 19–58 [IAS Special Publication]. https://doi.org/10.1002/9781118920435.ch2

McKie, T., 2017. Palaeogeographic evolution of latest Permian and Triassic salt basins in Northwest Europe. In: Soto, J. I., Flinch, J. F. and Tari, G. (eds.) *Permo-triassic salt provinces of Europe, North Africa and the Atlantic margins* (pp. 159-173). Elsevier. https://doi.org/10.1016/B978-0-12-809417-4.00008-2

McKie, T. and Williams, B., 2009. Triassic palaeogeography and fluvial dispersal across the northwest European Basins. Geological Journal, 44(6), pp.711-741. https://doi.org/10.1002/gj.1201

Medici, G., West, L.J., Mountney, N.P. and Welch, M., 2019. Permeability of rock discontinuities and faults in the Triassic Sherwood Sandstone Group (UK): insights for management of fluvio-aeolian aquifers worldwide. Hydrogeology Journal, 27(8), pp.2835-2855. https://doi.org/10.1007/s10040-019-02035-7

Meijer, N., Licht, A., Woutersen, A., Hoorn, C., Robin-Champigneul, F., Rohrmann, A., Tagliavento, M., Brugger, J., Kelemen, F.D., Schauer, A.J. and Hren, M.T., 2024. Proto-monsoon rainfall and greening in Central Asia due to extreme early Eocene warmth. *Nature Geoscience*, *17*(2), pp.158-164. https://doi.org/10.1038/s41561-023-01371-4

Meinshausen, M., Smith, S.J., Calvin, K., Daniel, J.S., Kainuma, M.L., Lamarque, J.F., Matsumoto, K., Montzka, S.A., Raper, S.C., Riahi, K. and Thomson, A.G.J.M.V., 2011. The RCP greenhouse gas concentrations and their extensions from 1765 to 2300. Climatic change, 109(1), p.213. https://doi.org/10.1007/s10584-011-0156-z

Menacherry, S., Kaldi, J., Lang, S. and Payenberg, T., 2009. PS Suitability of the Dryland Fluvial-Aeolian Sediments and Its Depositional System for CO2 Sequestration, Analogues Study from Umbum Creek, Lake Eyre, Central Australia. Presented at the AAPG International Conference and Exhibition, AAPG Search and Discovery, Cape Town, South Africa (2009), pp. 1-14

Meyer-Peter, E., and R. Müller. 1948. Formulas for Bed-Load Transport.

Miall, A.D. 1994. Reconstructing fluvial macroform architecture from two-dimensional outcrops; examples from the Castlegate Sandstone, Book Cliffs, Utah. Journal of Sedimentary Research, v. 64, p. 146-158.

Miall, A.D., 2006. The geology of fluvial deposits: sedimentary facies, basin analysis, and petroleum geology. Springer.

Mijnlieff, H.F., 2020. Introduction to the geothermal play and reservoir geology of the Netherlands. *Netherlands Journal of Geosciences*, *99*, p.e2. https://doi.org/10.1017/njg.2020.2

Millennium Ecosystem Assessment, 2005. Ecosystems and human well-being: wetlands and water synthesis. World Resources Institute, Washington, DC.

Morón, S., Amos, K. and Mann, S., 2014. Fluvial reservoirs in dryland endorheic basins: the Lake Eyre Basin as a world-class modern analogue. *The APPEA Journal*, *54*(1), pp.119-134. https://doi.org/10.1071/AJ13014

Morton, A., Hounslow, M.W. and Frei, D., 2013. Heavy-mineral, mineral-chemical and zircon-age constraints on the provenance of Triassic sandstones from the Devon coast, southern Britain. *Geologos*, *19*(1-2), pp.67-85. https://doi.org/10.2478/logos-2013-0005

Morton, A., Knox, R. and Frei, D., 2016. Heavy mineral and zircon age constraints on provenance of the Sherwood Sandstone Group (Triassic) in the eastern Wessex Basin, UK. *Proceedings of the Geologists' Association*, *127*(4), pp.514-526. https://doi.org/10.1016/j.pgeola.2016.06.001

Moscardini, R.I., English, K.L., Raine, R., Haughton, P.D., English, J.M. and Cooper, M., 2025. Reservoir heterogeneity in the Triassic Sherwood Sandstone Group: new insights from the Larne Basin, Northern Ireland. *Geoenergy*, *3*(1), pp.geoenergy2025-015. https://doi.org/10.1144/geoenergy2025-015

Nanson, G.C. and Huang, H.Q., 2017. Self-adjustment in rivers: Evidence for least action as the primary control of alluvial-channel form and process. Earth Surface Processes and Landforms, 42(4), pp.575-594. https://doi.org/10.1002/esp.3999

Nanson, G.C. and Knighton, A.D., 1996. Anabranching rivers: their cause, character and classification. *Earth surface processes and landforms*, *21*(3), pp.217-239. https://doi.org/10.1002/(SICI)1096-9837(199603)21:3%3C217::AID-ESP611%3E3.0.CO;2-U

Newell, A. J., 2017a. Rifts, rivers and climate recovery: A new model for the Triassic of England. *Proceedings of the Geologists' Association*, *129*(3), pp.352-371. https://doi.org/10.1016/j.pgeola.2017.04.001

Newell, A. J., 2017b. Evolving stratigraphy of a Middle Triassic fluvial-dominated sheet sandstone: The Otter Sandstone Formation of the Wessex Basin (UK). *Geological Journal*, *53*(5), pp.1954-1972. https://doi.org/10.1002/gj.3026

Newell, A. J., 2023 *The Sherwood Sandstone and Bacton groups of the East Midlands Shelf – an onshore to offshore correlation using outcrop evidence and geophysical logs.* Nottingham, UK, British Geological Survey.

Newell, A.J. and Shariatipour, S.M., 2016. Linking outcrop analogue with flow simulation to reduce uncertainty in sub-surface carbon capture and storage: an example from the Sherwood Sandstone Group of the Wessex Basin, UK. *Geological Society, London, Special Publications*, *436*(1), pp.231-246. https://doi.org/10.1144/SP436

Newell, A J, Smith, N J., 2009. Bromsgrove Aquifer Groundwater Modelling Study: Results from Task 1.1 3D Visualisation and Geological Framework of the Bromsgrove Aquifer. British Geological Survey Commissioned Report, CR/09/023. 18pp.

North, C.P., Nanson, G.C. and Fagan, S.D., 2007. Recognition of the sedimentary architecture of dryland anabranching (anastomosing) rivers. *Journal of Sedimentary Research*, *77*(11), pp.925-938. https://doi.org/10.2110/jsr.2007.089

Nyberg, B., Helland-Hansen, W., Gawthorpe, R.L., Sandbakken, P., Eide, C.H., Sømme, T., Hadler-Jacobsen, F. and Leiknes, S., 2018. Revisiting morphological relationships of modern source-to-sink segments as a first-order approach to scale ancient sedimentary systems. *Sedimentary Geology*, *373*, pp.111-133. https://doi.org/10.1016/j.sedgeo.2018.06.007

Ogg, J. G., Chen, Z.-Q., Orchard, M. J., Jiang, H. S., 2020. Chapter 25 - The Triassic Period. In: Gradstein, F. M., Ogg, J. G., Schmitz, M. D., Ogg G. M., Geologic Time Scale, (pp. 903-953) Elsevier, https://doi.org/10.1016/B978-0-12-824360-2.00025-5.

Paola, C. and Borgman, L., 1991. Reconstructing random topography from preserved stratification. Sedimentology, 38(4), pp.553-565. https://doi.org/10.1111/j.1365-3091.1991.tb01008.x

Plink-Björklund, P., 2015. Morphodynamics of rivers strongly affected by monsoon precipitation: review of depositional style and forcing factors. *Sedimentary Geology*, *323*, pp.110-147. https://doi.org/10.1016/j.sedgeo.2015.04.004

Parker, G., 1976. On the cause and characteristic scales of meandering and braiding in rivers. Journal of fluid mechanics, 76(3), pp.457-480. https://doi.org/10.1017/S0022112076000748

Piedrahita, V.A., Heslop, D., Roberts, A.P., Rohling, E.J., Galeotti, S., Florindo, F. and Li, J., 2025. Assessing the duration of the Paleocene-Eocene Thermal Maximum. *Geophysical Research Letters*, *52*(7), p.e2024GL113117. https://doi.org/10.1029/2024GL113117

Plant, J. A., Jones, D. G., and Haslam, H W (editors). 1999. The Cheshire Basin: Basin evolution, fluid movement and mineral resources in a Permo-Triassic rift setting. Keyworth, Nottingham: for the British Geological Survey.

Van Praagh, C.J., Webb, J.A. and White, S.Q., 2024. The White Hills Gravel of central Victoria: an anomalous Paleogene very coarse-grained fluvial deposit. *Australian Journal of Earth Sciences*, *71*(6), pp.757-777. https://doi.org/10.1080/08120099.2024.2388575

Prieur, M., Robin, C., Braun, J., Vaucher, R., Whittaker, A.C., Jaimes-Gutierrez, R., Wild, A., McLeod, J.S., Malatesta, L., Fillon, C. and Schlunegger, F., 2025. Climate control on erosion: Evolution of sediment flux from mountainous catchments during a global warming event, PETM, Southern Pyrenees, Spain. Geophysical Research Letters, 52(7), p.e2024GL112404. https://doi.org/10.1029/2024GL112404

Purvis, K. and Wright, V.P., 1991. Calcretes related to phreatophytic vegetation from the Middle Triassic Otter Sandstone of south west England. *Sedimentology*, *38*(3), pp.539-551. https://doi.org/10.1111/j.1365-3091.1991.tb00366.x

Radley, J.D. and Coram, R.A., 2015. Derived Skolithos pipe rock in the Budleigh Salterton Pebble Beds (Early Triassic, East Devon, UK). Proceedings of the Geologists' Association, 126(2), pp.220-225. http://dx.doi.org/10.1016/j.pgeola.2014.10.007

Radley, J.D. and Coram, R.A., 2016. The Chester Formation (Early Triassic, southern Britain): sedimentary response to extreme greenhouse climate?. *Proceedings of the Geologists' Association*, *127*(5), pp.552-557. http://dx.doi.org/10.1016/j.pgeola.2016.08.002

Ramos, A. and Sopeña, A., 1983. Gravel bars in low-sinuosity streams (Permian and Triassic, central Spain). *Modern and ancient fluvial systems*, pp.301-312. https://doi.org/10.1002/9781444303773.ch24

Ravidà, D.C., Caracciolo, L., Heins, W.A. and Stollhofen, H., 2021. Reconstructing environmental signals across the Permian-Triassic boundary in the SE Germanic basin: Palaeodrainage modelling and quantification of sediment flux. *Global and Planetary Change*, *206*, p.103632. https://doi.org/10.1016/j.gloplacha.2021.103631

Rees, J G, and Wilson, A A. 1998. Geology of the country around Stoke-on-Trent. Memoir of the Geological Survey, Sheet 123 (England and Wales).

Reynolds, T., 2024. Grain size from source to sink–modern and ancient fining rates. *Earth-Science Reviews*, *250*, p.104699. https://doi.org/10.1016/j.earscirev.2024.104699

Romans, B. W., Castelltort, S., Covault, J. A., Fildani, A. & Walsh, J. P. (2016) Environmental signal propagation in sedimentary systems across timescales. *Earth Science Reviews*. 153, 7-29. 10.1016/j.earscirev.2015.07.012

Safriel, U, Adeel, Z, Niemeijer, D, Puigdefabregas, J, White, R, Lal, R, Winslow, M, Ziedler, J, Prince, S, Archer, E & King, C 2005, Dryland Systems. in R Hassan, R Scholes & N Ash (eds), Ecosystems and human well-being: current state and trends. Island Press, Washington, pp. 623-662.

Satoh, Y., Yoshimura, K., Pokhrel, Y. et al. The timing of unprecedented hydrological drought under climate change. Nature Communications 13, 3287 (2022). https://doi.org/10.1038/s41467-022-30729-2

Sharma, N., Whittaker, A.C., Watkins, S.E., Valero, L., Vérité, J., Puigdefabregas, C., Adatte, T., Garcés, M., Guillocheau, F. and Castelltort, S., 2023. Water discharge variations control fluvial stratigraphic architecture in the Middle Eocene Escanilla formation, Spain. Scientific Reports, 13(1), p.6834. https://doi.org/10.1038/s41598-023-33600-6

Schellschmidt, R., Sanner, B., Pester, S. and Schulz, R., 2010, April. Geothermal energy use in Germany. In Proceedings world geothermal congress (Vol. 152, p. 19).

Schmitz, B. and Pujalte, V., 2007. Abrupt increase in seasonal extreme precipitation at the Paleocene-Eocene boundary. *Geology*, *35*(3), pp.215-218. https://doi.org/10.1130/G23261A.1

Selwood, E.B., Edwards, R.A., Simpson, S., Chesher, J.A., Hamblin, R.J.O., Henson, M.R., Riddolls, B.W. and Waters, R.A., 1984. Geology of the country around Newton Abbot. Memoir for 1:50,000 geological sheet 339, New Series.

Sendino, C., Taylor, P.D. and Van Iten, H., 2012. Metaconularia? pyramidata (Bronn, 1837): a scyphozoan from the Ordovician of Normandy, France, recorded for the first time as a reworked fossil in the Triassic of Devon, England. *Geodiversitas*, *34*(2), pp.283-296. http://dx.doi.org/10.5252/g2012n2a3

Smith, S.A., 1990. The sedimentology and accretionary styles of an ancient gravel-bed stream: the Budleigh Salterton Pebble Beds (Lower Triassic), southwest England. *Sedimentary Geology*, *67*(3-4), pp.199-219. https://doi.org/10.1016/0037-0738(90)90035-R

Smith, S.A. and Edwards, R.A., 1991. Regional sedimentological variations in Lower Triassic fluvial conglomerates (Budleigh Salterton Pebble Beds), southwest England: some implications for palaeogeography and basin evolution. *Geological Journal*, *26*(1), pp.65-83. https://doi.org/10.1002/gj.3350260105

Steel, R.J. and Thompson, D.B., 1983. Structures and textures in Triassic braided stream conglomerates (‘Bunter’pebble beds) in the Sherwood Sandstone Group, North Staffordshire, England. Sedimentology, 30(3), pp.341-367. https://doi.org/10.1111/j.1365-3091.1983.tb00677.x

Sun, Y., Joachimski, M.M., Wignall, P.B., Yan, C., Chen, Y., Jiang, H., Wang, L. and Lai, X., 2012. Lethally hot temperatures during the Early Triassic greenhouse. *Science*, *338*(6105), pp.366-370. https://www.science.org/doi/10.1126/science.1224126

Svendsen, J.B. and Hartley, N.R., 2001. Comparison between outcrop-spectral gamma ray logging and whole rock geochemistry: implications for quantitative reservoir characterisation in continental sequences. *Marine and Petroleum Geology*, *18*(6), pp.657-670. https://doi.org/10.1016/S0264-8172(01)00022-8

Tooth, S. and Nanson, G.C., 1999. Anabranching rivers on the Northern Plains of arid central Australia. Geomorphology, 29(3-4), pp.211-233. https://doi.org/10.1016/S0169-555X(99)00021-5

Tooth, S. and Nanson, G.C., 2000. The role of vegetation in the formation of anabranching channels in an ephemeral river, Northern plains, arid central Australia. Hydrological processes, 14(16-17), pp.3099-3117. https://doi.org/10.1002/1099-1085(200011/12)14:16/17%3C3099::AID-HYP136%3E3.0.CO;2-4

Tooth, S. and Nanson, G.C., 2004. Forms and processes of two highly contrasting rivers in arid central Australia, and the implications for channel-pattern discrimination and prediction. Geological Society of America Bulletin, 116(7-8), pp.802-816. https://doi.org/10.1130/B25308.1

Trampush, S.M., Huzurbazar, S. and McElroy, B., 2014. Empirical assessment of theory for bankfull characteristics of alluvial channels. Water Resources Research, 50(12), pp.9211-9220. https://doi.org/10.1002/2014WR015597

Tyrrell, S., Haughton, P.D., Souders, A.K., Daly, J.S. and Shannon, P.M., 2012. Large-scale, linked drainage systems in the NW European Triassic: insights from the Pb isotopic composition of detrital K-feldspar. *Journal of the Geological Society*, *169*(3), pp.279-295. https://doi.org/10.1144/0016-76492011-104

Valenza, J.M., Whittaker, A.C., Ganti, V., Greenberg, E., McLeod, J. and Wild, A.L., 2026. Pre-vegetation fluvial sheet sands explained: Bedform and bar architecture evidence for 1.2 Ga rapidly migrating, meandering, and high-sinuosity wandering rivers. Geology, 54(1), pp.30-34. https://doi.org/10.1130/G52858.1

Van Vuuren, D.P., O'Neill, B.C., Tebaldi, C., Sanderson, B.M., Chini, L.P., Friedlingstein, P., Hasegawa, T., Riahi, K., Govindasamy, B., Bauer, N. and Eyring, V., 2026. The scenario model intercomparison project for CMIP7 (ScenarioMIP-CMIP7). *Geoscientific Model Development*, *19*(7), pp.2627-2656. https://doi.org/10.5194/gmd-19-2627-2026

Wang, H., Liu, J., Klaar, M., Chen, A., Gudmundsson, L. and Holden, J., 2024. Anthropogenic climate change has influenced global river flow seasonality. *Science*, *383*(6686), pp.1009-1014. https://doi.org/10.1126/science.adi9501

Wentworth, C. K. 1922. “A Scale of Grade and Class Terms for Clastic Sediments.” Journal of Geology 30: 377–392

Willard, D.A., Nelissen, M., Sluijs, A., Brinkhuis, H., Reichgelt, T., Robinson, M. and Self-Trail, J.M., 2026. Terrestrial ecosystem response to changing temperature and seasonality in the Paleocene-Eocene Thermal Maximum: Shallow marine records from the Salisbury Embayment, USA. *Paleoceanography and Paleoclimatology*, *41*(3), p.e2025PA005278. https://doi.org/10.1029/2025PA005278

Wills, L. J. (1956). Concealed coalfields: a palaeographical study of the stratigraphy and tectonics of mid-England in relation to coal reserves. London: Blackie.

Wills, L.J., 1970. The Triassic succession in the central Midlands in its regional setting. *Quarterly Journal of the Geological Society*, *126*(1-4), pp.225-283. https://doi.org/10.1144/gsjgs.126.1.0225

Whittaker, A.C., Duller, R.A., Springett, J., Smithells, R.A., Whitchurch, A.L. and Allen, P.A., 2011. Decoding downstream trends in stratigraphic grain size as a function of tectonic subsidence and sediment supply. *Bulletin*, *123*(7-8), pp.1363-1382. https://doi.org/10.1130/B30351.1

Wolman, M. G. 1954. “A Method of Sampling Coarse River-Bed Material.” Eos, Transactions American Geophysical Union 35: 951–956.

Wong, M. and Parker, G., 2006. Reanalysis and correction of bed-load relation of Meyer-Peter and Müller using their own database. Journal of hydraulic engineering, 132(11), pp.1159-1168. https://doi.org/10.1061/(ASCE)0733-9429(2006)132:11(1159)

Wood, J., McLeod, J.S., Lyster, S.J. and Whittaker, A.C., 2023. Rivers of the Variscan Foreland: fluvial morphodynamics in the Pennant Formation of South Wales, UK. *Journal of the Geological Society*, *180*(1), pp.jgs2022-048. https://doi.org/10.1144/jgs2022-048

Wood, J., J. S. McLeod, S. J. Lyster, and A. C. Whittaker. 2025. “Reply to Comment on Rivers of the Variscan Foreland: Fluvial Morphodynamics in the Pennant Formation of South Wales, UK.” Journal of the Geological Society 182: jgs2025-087.

Wood, J., McLeod, J.S., Lyster, S.J. and Whittaker, A.C., 2025. Reply to comment on ‘Rivers of the Variscan Foreland: fluvial morphodynamics in the Pennant Formation of South Wales, UK’. *Journal of the Geological Society*, *182*(5), pp.jgs2025-087. https://doi.org/10.1144/jgs2025-087

Wright, V.P., Marriott, S.B. and Vanstone, S.D., 1991. A ‘reg’palaeosol from the Lower Triassic of south Devon: stratigraphic and palaeoclimatic implications. *Geological Magazine*, *128*(5), pp.517-523. https://doi.org/10.1017/S0016756800018653

Yan, X., Hampson, G.J. and Whittaker, A.C., 2026. A new source-to-sink synthesis of the Middle Triassic Helsby Sandstone Formation (Sherwood Sandstone Group) river system of the British Isles. Journal of the Geological Society, pp.jgs2025-214. https://doi.org/10.1144/jgs2025-214

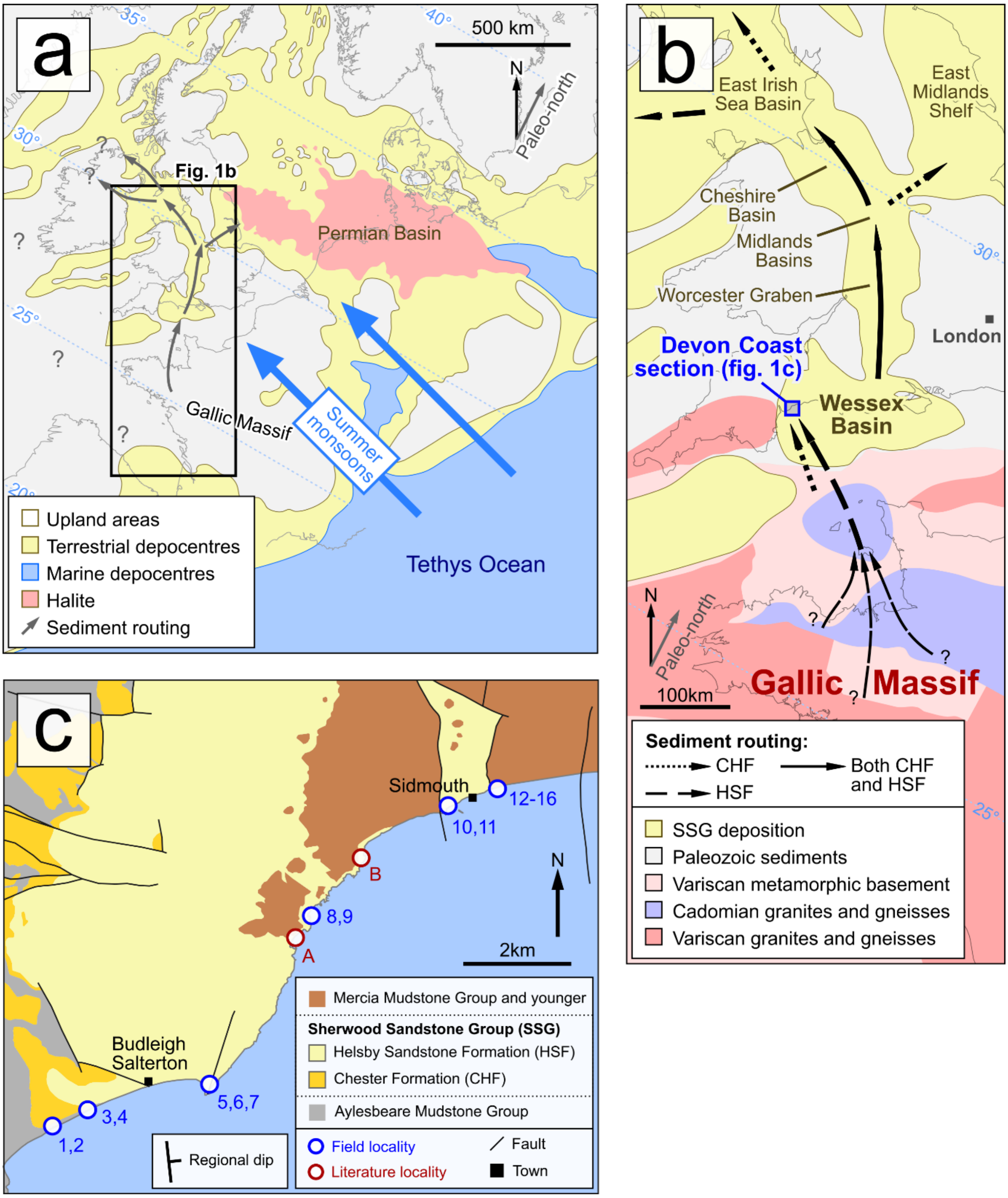

Figure 1: a) Paleogeography of NW Europe during the early to mid-Triassic (adapted from McKie, 2017; Yan et al., 2026). **b)** early to mid-Triassic sediment routing across north France and the British Isles (Burgess et al., 2025; Yan et al., 2026). **c)** Field localities and distribution of the Sherwood Sandstone Group at outcrop in the Devon study area. Locality A: Lorsong and Atkinson (1994), B: Newell and Shariatipour, 2016. CM: Cornubian Massif, EISB: East Irish Sea Basin, WB: Wessex Basin. **c)** Geological Map Data BGS © UKRI 2025.

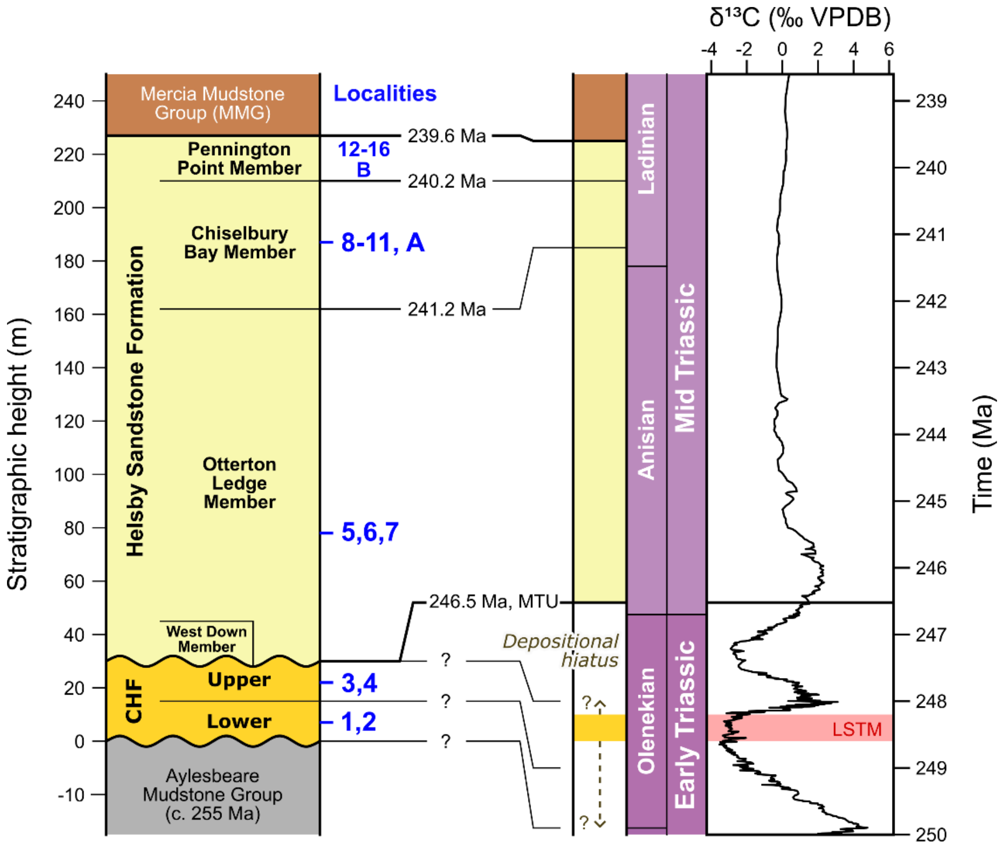

Figure 2: Lithostratigraphy (Smith and Edwards, 1991; Newell, 2017b) and chronostratigraphy (Hounslow and McIntosh, 2003; Hounslow et al., 2017; Hounslow and Gallois, 2023; Yan et al., 2026) for the Devon coastal outcrop section, plotted with the global δ¹³C isotope curve (Sun et al., 2012; Ogg et al., 2020). LSTM: Late Smithian Thermal Maximum, MTU: Mid-Triassic Unconformity, VPDB: Vienna Peedee Belemnite. Localities are the same as in **fig. 1c.**

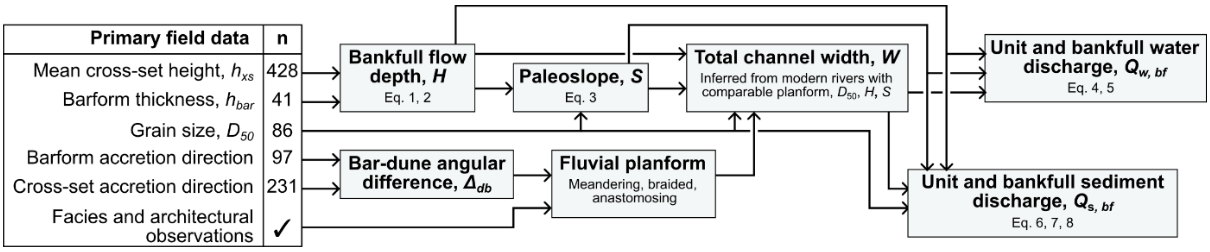

Figure 3: Data analysis flowchart showing the relationship between primary field data and the derivation of key results.

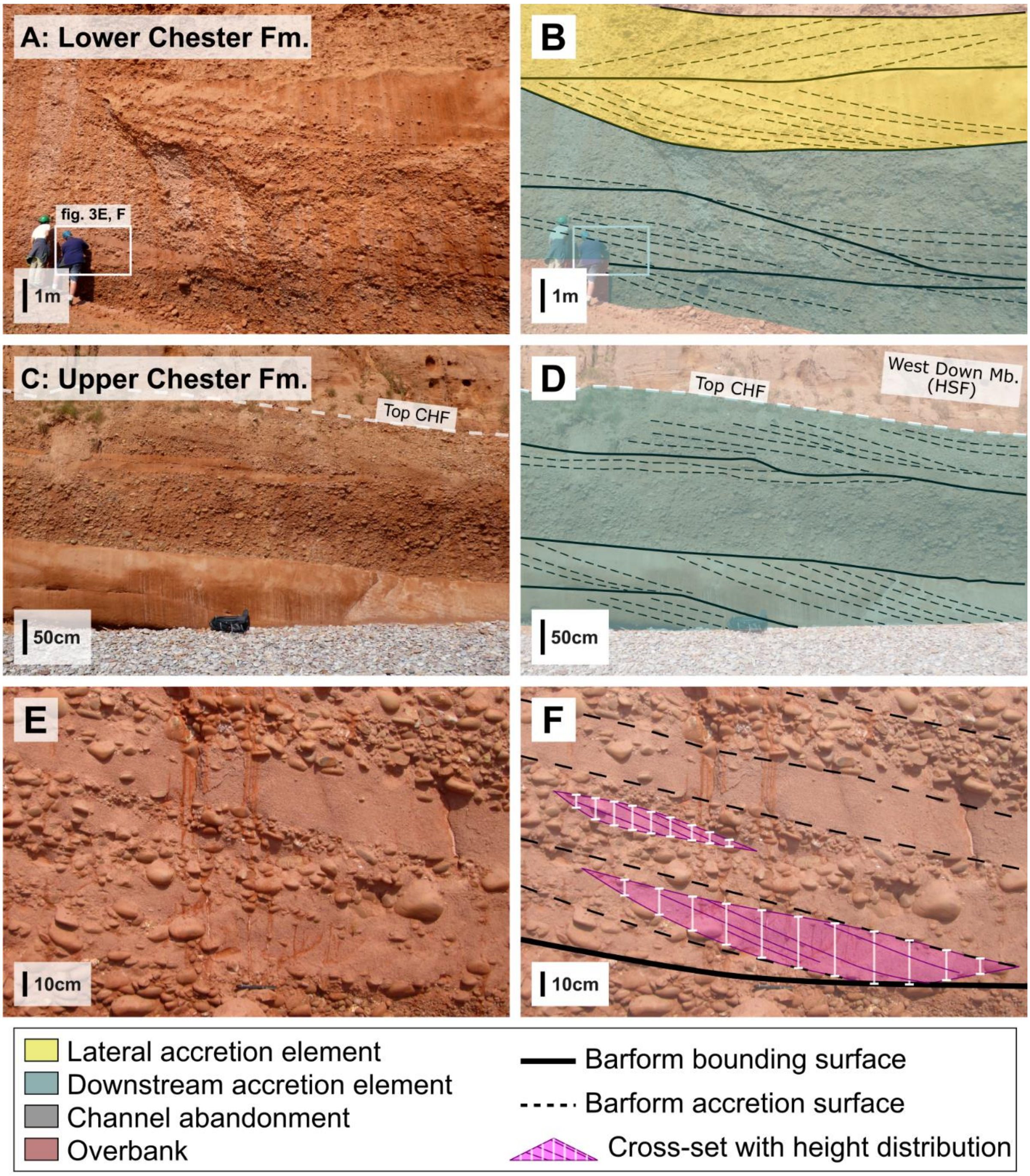

Fig. 4: Representative outcrop photographs of the **a, b)** lower and **c, d)** upper Chester Formation at localities 1 and 4, respectively (**fig. 1c**), with interpreted architectural elements. Note the change in scale. **e, f)** cross-sets in the Chester Formation showing measured height distributions.

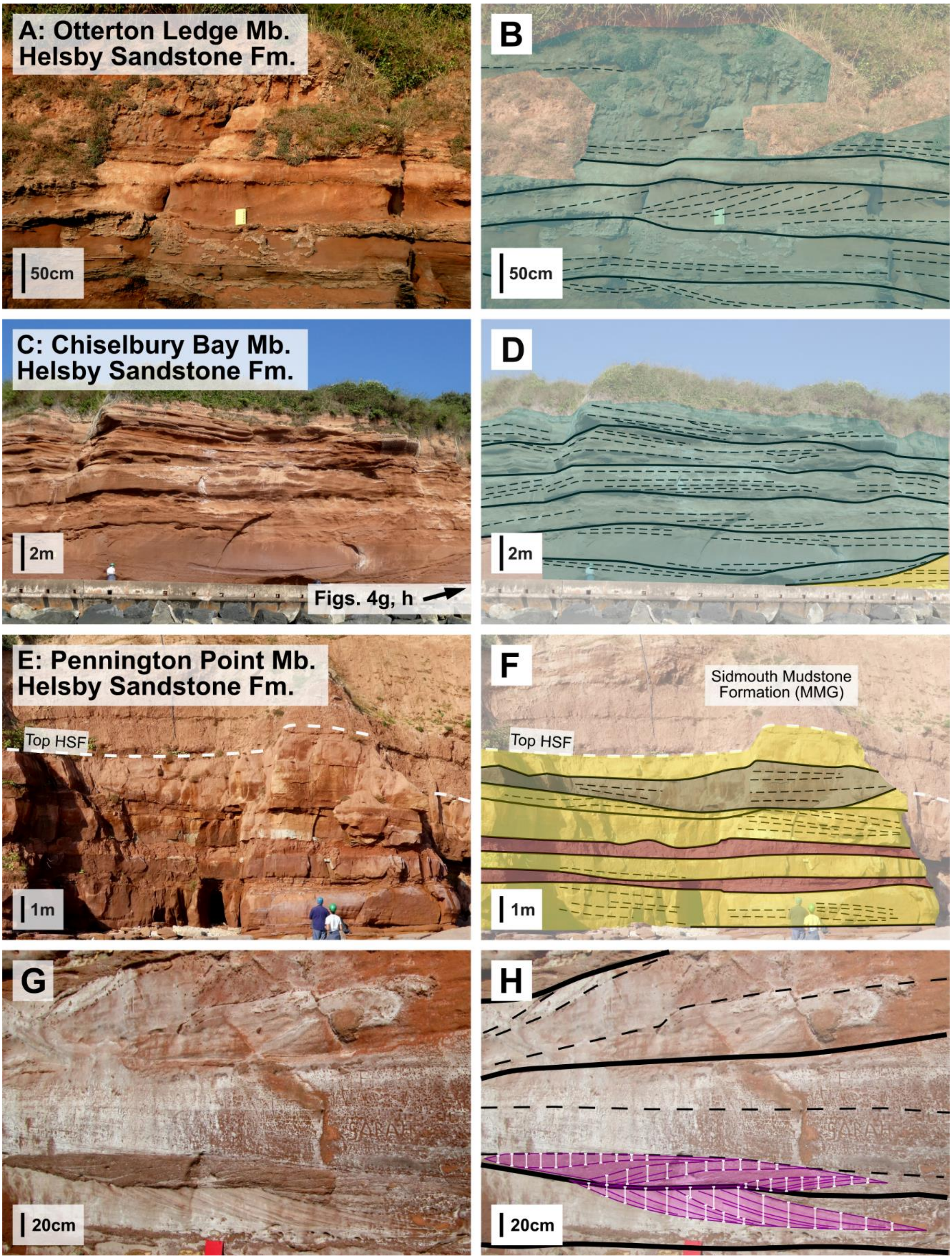

Fig. 5: Representative outcrop photographs of the Helsby Sandstone Formation (HSF) for the **a, b)** Otterton Ledge Member, **c, d)** Chiselbury Bay Member, and **e, f)** Pennington Point Member at localities 6, 10 and 15, respectively (**fig. 1c**), with interpreted architectural elements. Note the changes in scale. **g, h)** cross-sets in the HSF showing measured height distributions. For clarity, not all cross-sets are annotated. See **fig. 3** for key.

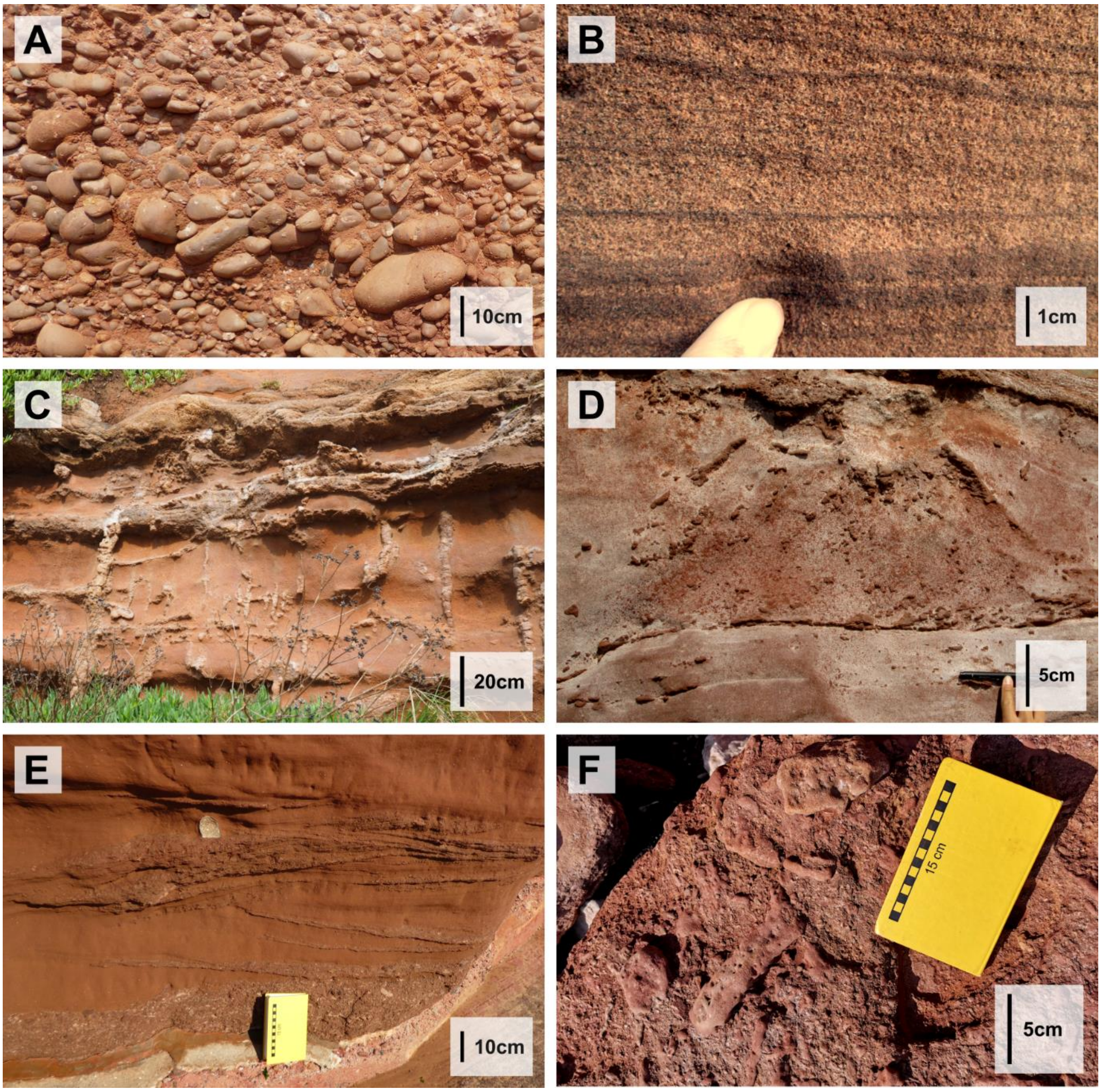

Figure 6: Representative grain size in the **a)** conglomeratic Chester Formation, **b)** sandstone-dominated Helsby Sandstone Formation (HSF) at localities 1 and 8, respectively (**fig. 1c**). In-situ rhizocretions in the **c)** Otterton Ledge Member, and **d)** Chiselbury Bay Member of the HSF at localities 6 and 11, respectively (**fig. 1c**). Rhizocretions reworked and deposited as gravel lags in the **e)** Chiselbury Bay Member, and **f)** Pennington Point Member of the HSF at localities 11 and 13, respectively (**fig. 1c**).

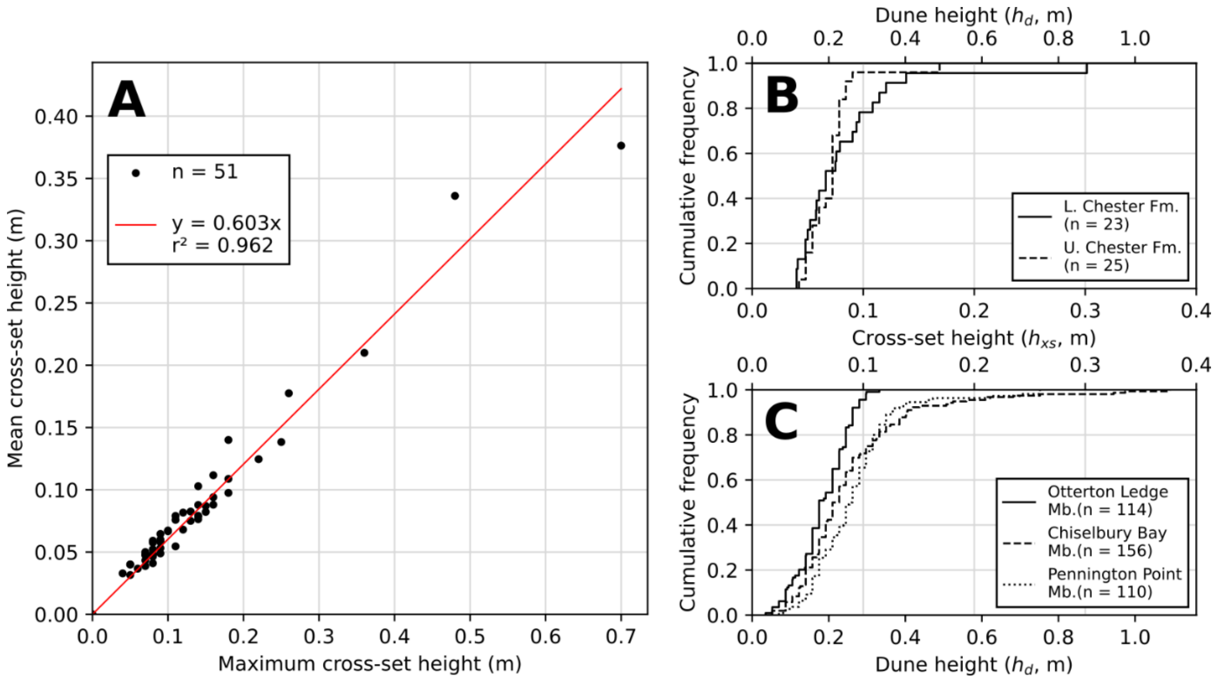

Figure 7: (a) Relationship between mean and maximum cross-set height for measured cross-sets in the Sherwood Sandstone Group. Trend line is derived from linear regression through point (0, 0). Cumulative frequency distribution of mean cross-set heights for the (**b**) Chester Formation, (**c**) Helsby Sandstone Formation.

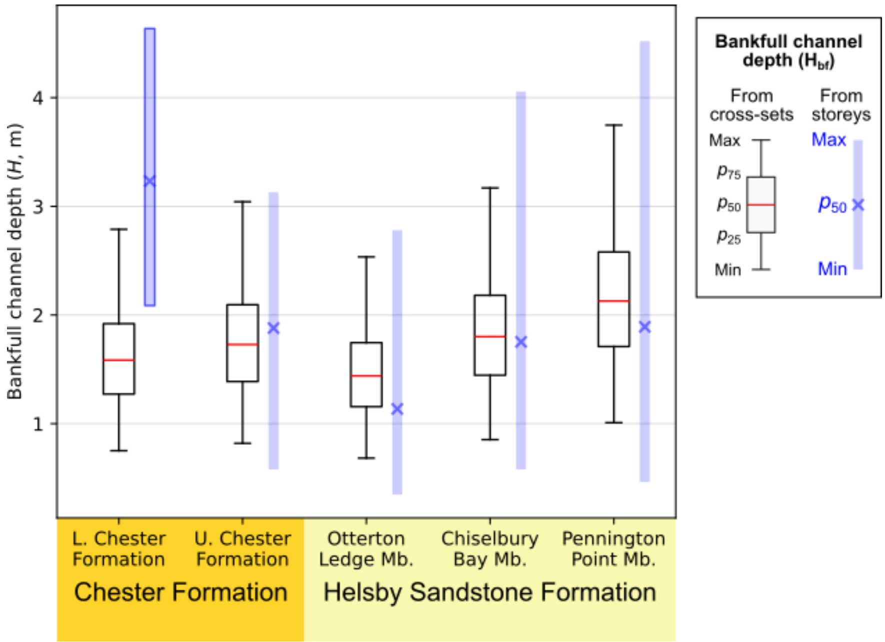

Figure 8: Bankfull flow depth for each lithostratigraphic member of the Chester Formation and Helsby Sandstone Formation, reconstructed by bedform and barform approaches.

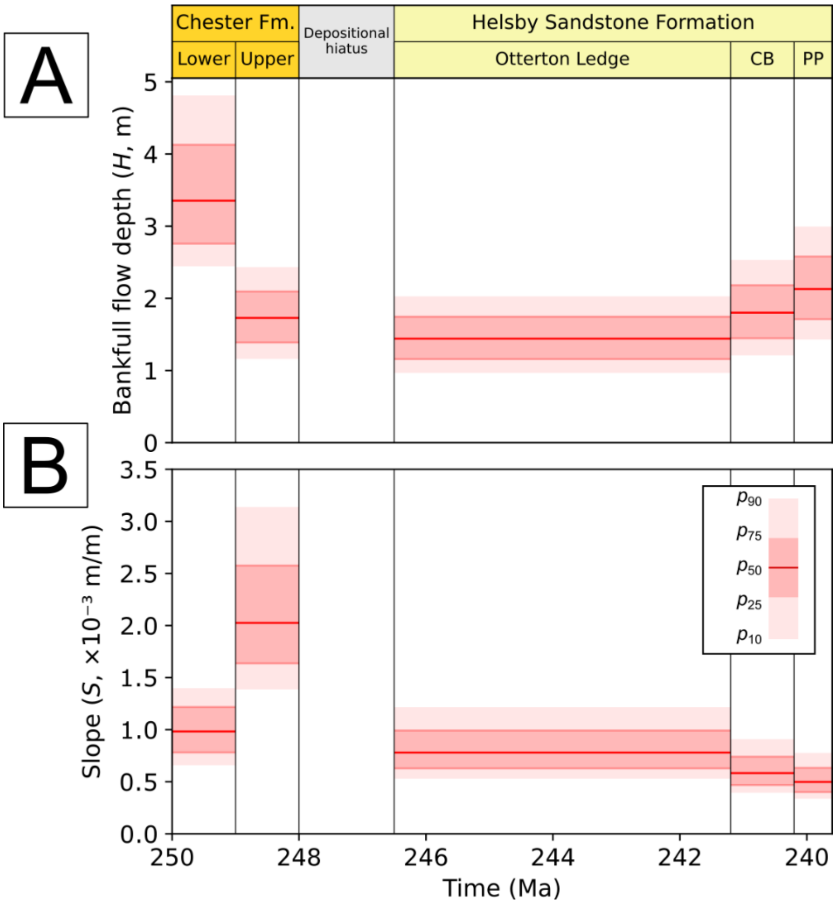

Figure 9: Temporal evolution of **a**) estimated bankfull flow depth, **b**) estimated slope. CB: Chiselbury Bay Member, PP: Pennington Point Member.

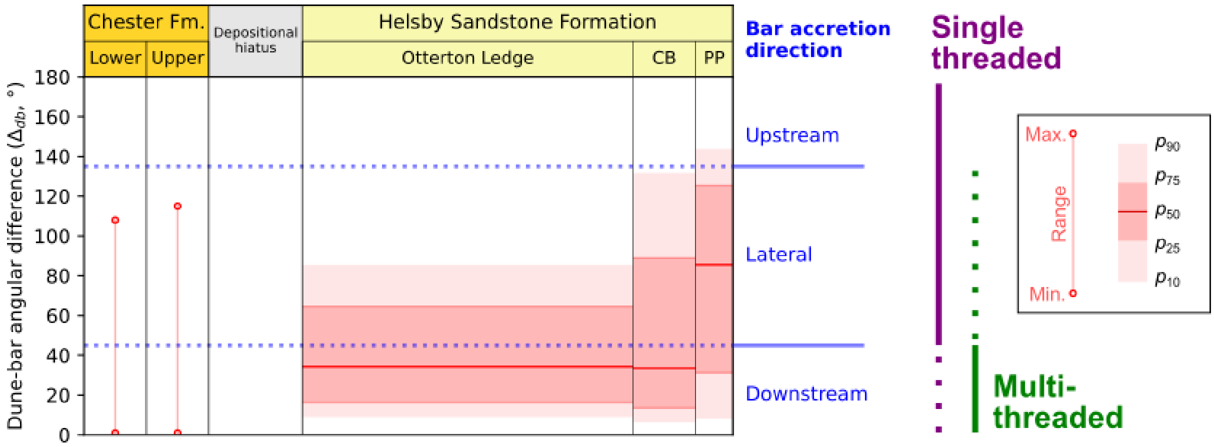

Figure 10: Plot of dune-bar angular difference, a planform-diagnostic parameter, plotted for the Sherwood Sandstone Group.

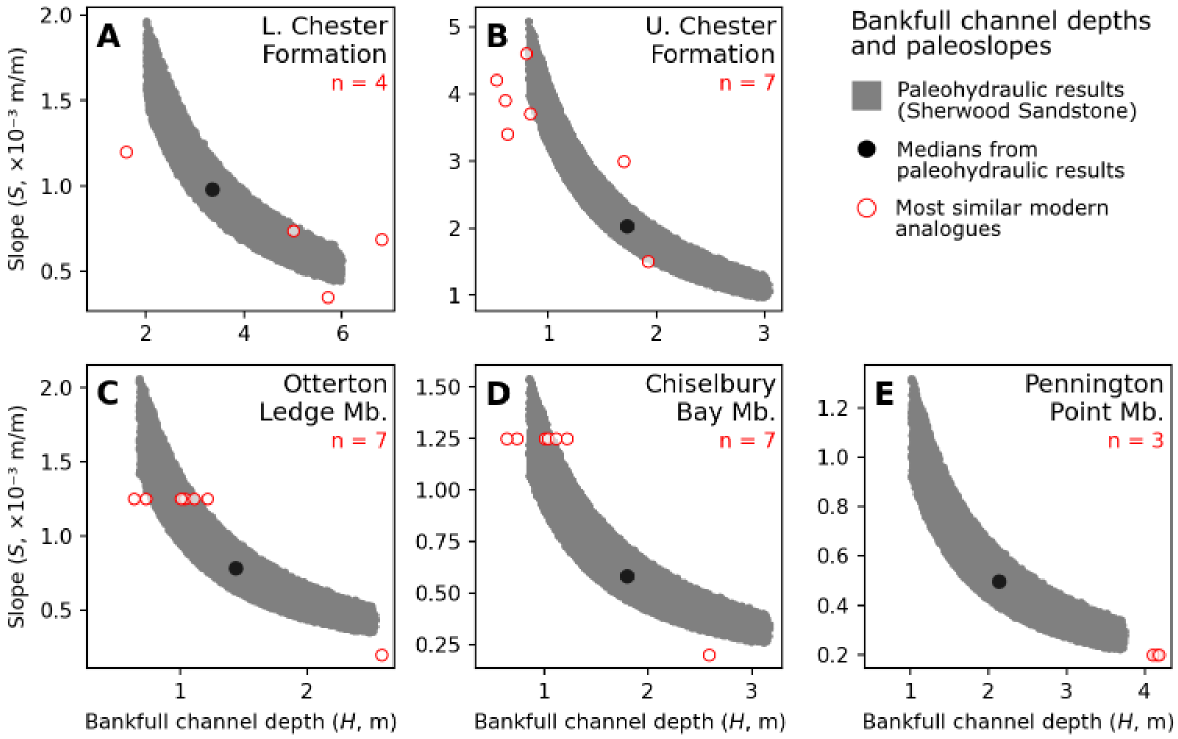

Figure 11 (a-e): Estimated values of slope and channel depth plotted for each stratigraphic division of the SSG (n = 10^5), compared to equivalent parameters in modern rivers of the same bed grain size and planform (Tooth and Nanson, 2004; Brunner, 2013; Nanson and Huang, 2017; Lyster et al., 2022).

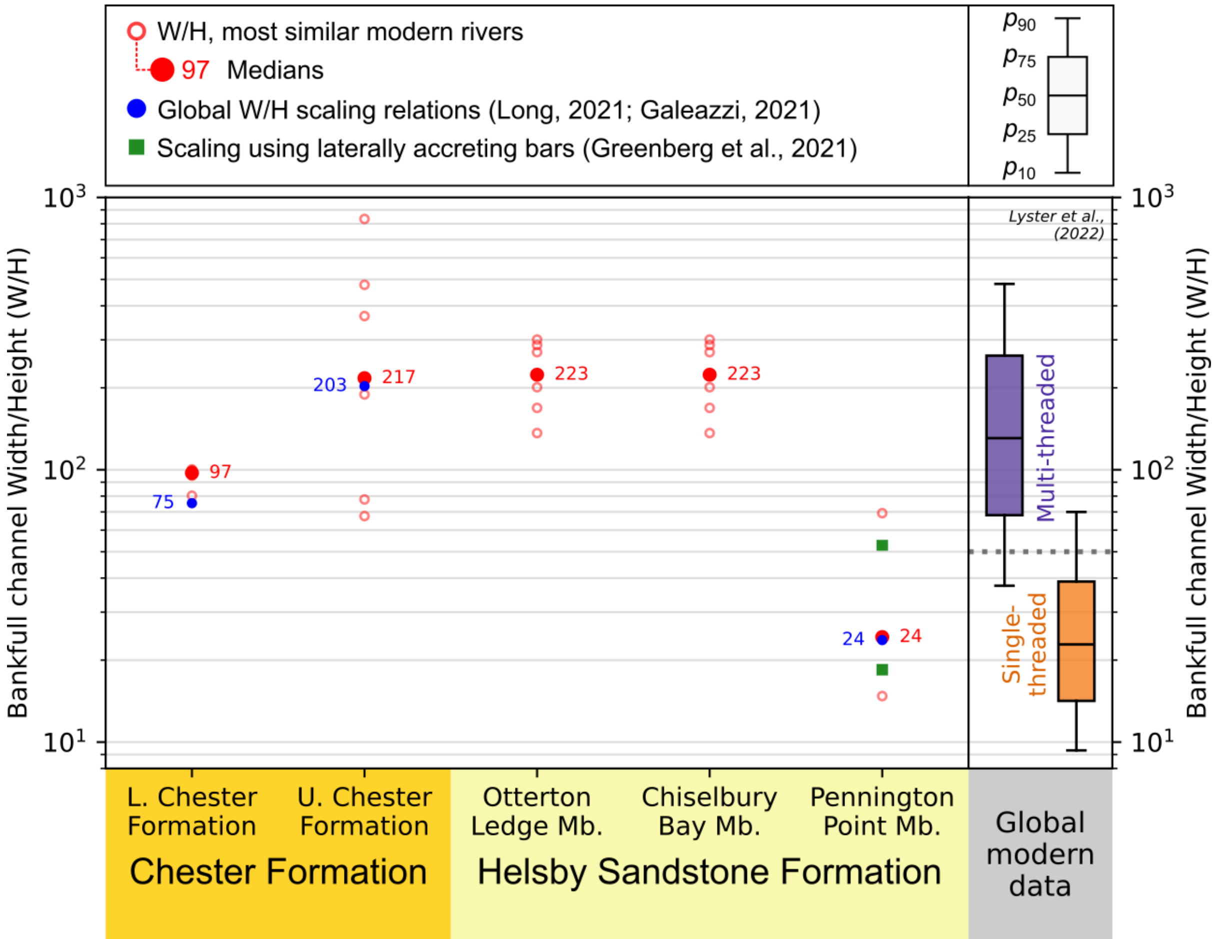

Figure 12: Inferred channel width/depth ratios (W/H) for each division of the Sherwood Sandstone Group, derived using three approaches. W/H is plotted for gemorphically similar modern rivers, which are identified using data in **fig. 11**. Scaling relationships of Long (2021) and Galeazzi (2022) are compiled from global datasets of channel height-width relationships, and channel count, respectively. The scaling relationship of Greenberg et al. (2022) uses laterally accreting bars. These data are compared to a global dataset of modern multithreaded and single-threaded rivers (Lyster et al., 2022). The grey dashed line correctly classifies 82% of modern single-threaded rivers, and 84% of modern multi-threaded rivers.

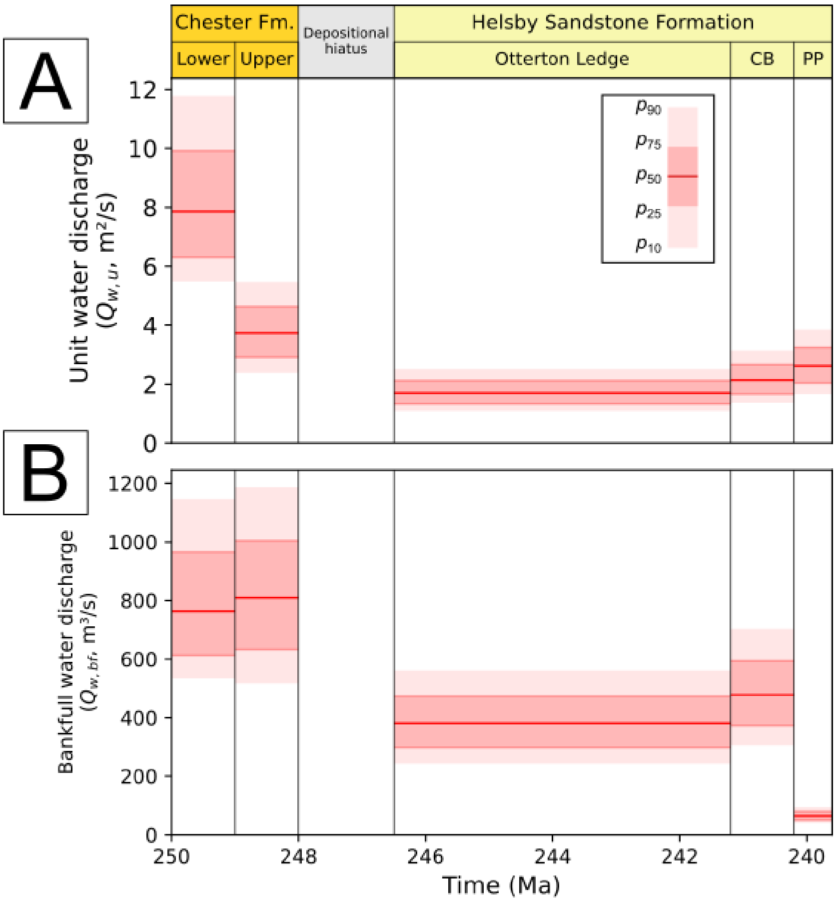

Figure 13: Temporal evolution of **a)** unit and **b)** bankfull water discharge. CB: Chiselbury Bay Member, PP: Pennington Point Member.

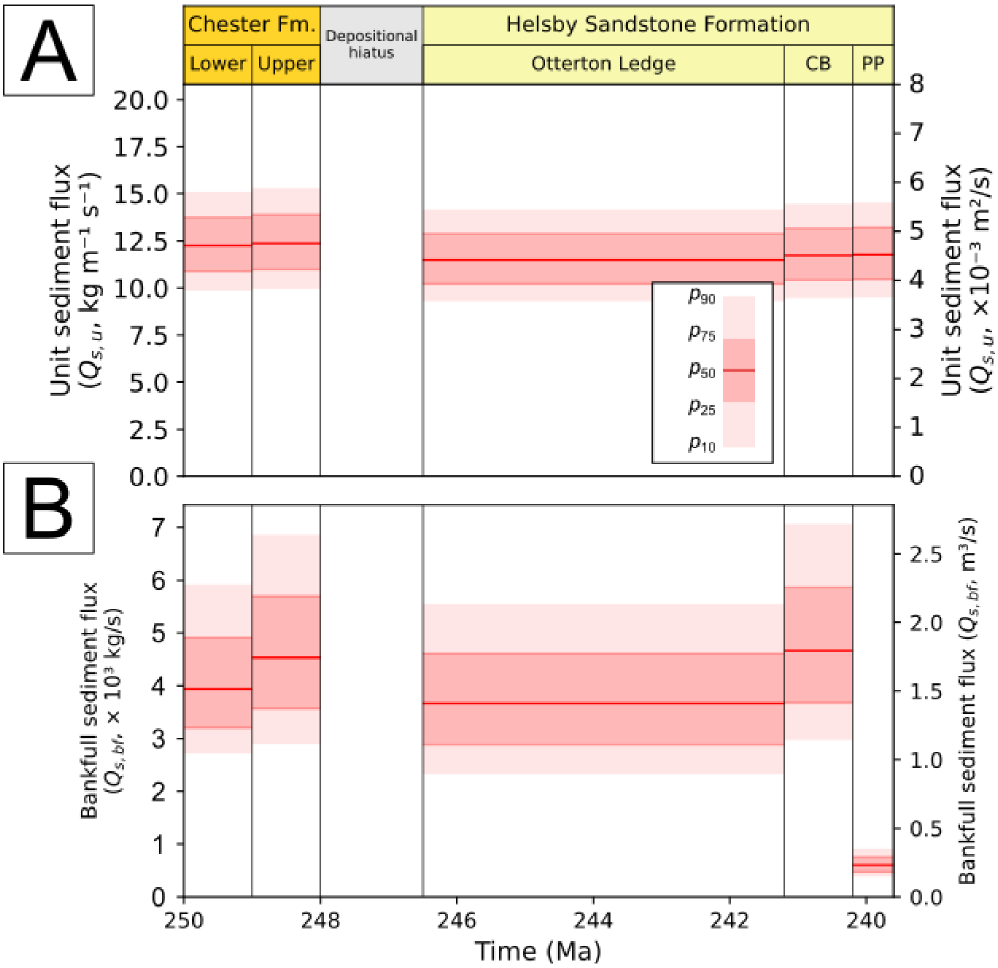

Figure 14: Temporal evolution of **a)** unit and **b)** bankfull sediment flux. CB: Chiselbury Bay Member, PP: Pennington Point Member.

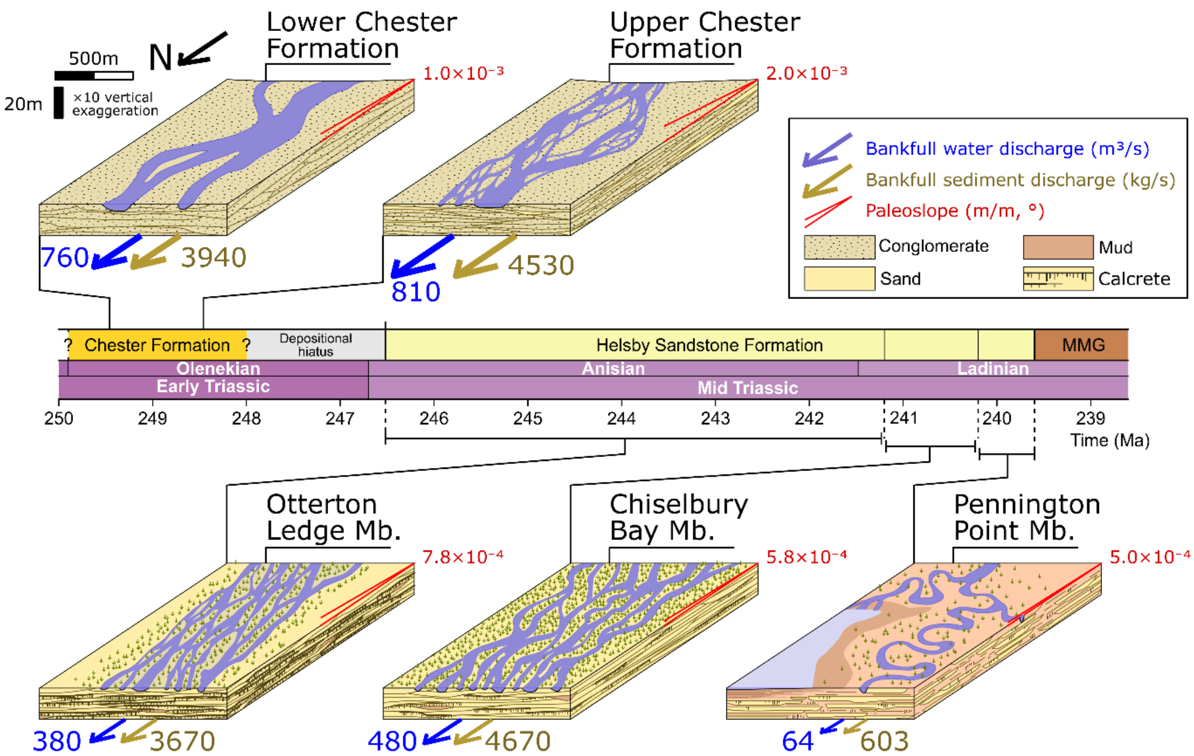

Figure 15: Block diagrams illustrating the temporal evolution of paleoslope, planform, architectural character, bankfull water discharge and bankfull sediment flux in rivers of the SSG in the Dorset coastal outcrops.

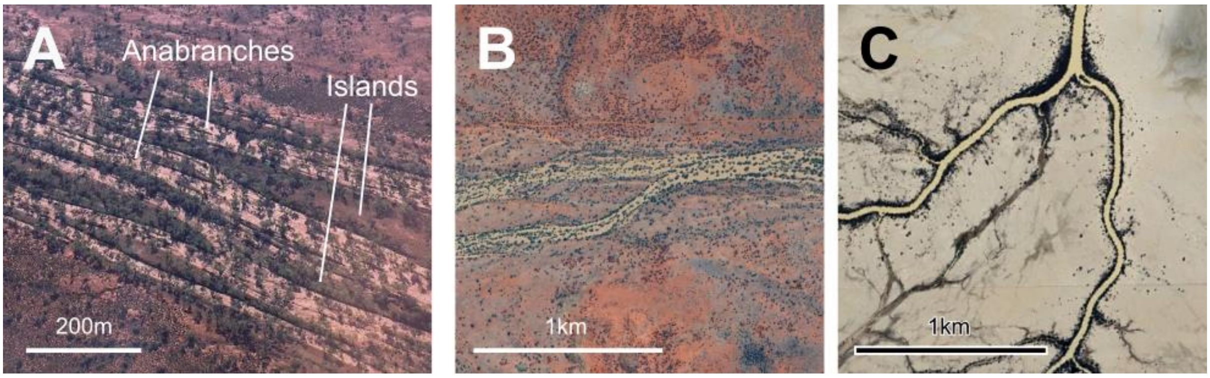

Figure 15: Climatically and geomorphically comparable modern river systems for the Helsby Sandstone Formation. **(a)** aerial and **(b)** satellite (-22.9078° S, 136.0472° E) views of the anastomosing, sand-bed Marshall River, Australia. **c)** satellite view of the sand-bed meandering distributary channels of the Diamantina River, Australia (-26.5672° S, 139.2516° E). **a)** from Tooth and Nanson (2000), **b)** and **c)** from Google imagery.